COMPUTATIONAL SCHEIMPFLUG IMAGING FOR IMPROVING DEPTH OF FIELD OF IRIS RECOGNITION SYSTEMS

Approved by:

_____

Dr. Marc P. Christensen, Professor

_____

Dr. Delores M. Etter, Professor

_____

Dr. Panos E. Papamichalis, Professor

_____

Dr. Dinesh Rajan, Professor

_____

Dr. Yunkai Zhou, Associate Professor

COMPUTATIONAL SCHEIMPFLUG IMAGING FOR IMPROVING DEPTH OF FIELD OF IRIS RECOGNITION SYSTEMS

A Dissertation Presented to the Graduate Faculty of

Bobby B. Lyle School of Engineering

Southern Methodist University

in

Partial Fulfillment of the Requirements

for the degree of

Doctor of Philosophy

with a

Major in Electrical Engineering

by

Indranil Sinharoy

(B.E. in Electronics & Communication Engineering, Visvesvaraya Tech. University, India, 2003)
(M.S. in Electrical Engineering, Southern Methodist University, 2006)

December 17, 2016

ACKNOWLEDGEMENTS

I would like to thank my advisor Dr. Marc P. Christensen for his relentless support and advise during the course of my Ph.D. study. His vision and experience influenced my work to a large degree. This is the end of Acknowledgement section.

Sinharoy, Indranil BE in Electronics & Communication Engineering, VTU, India, 2003
MS in Electrical Engineering, Southern Methodist University, 2006

Computational Scheimpflug Imaging for Improving
the Depth of Field of Iris Recognition Systems

Advisor: Professor Marc P. Christensen

Doctor of Philosophy December 17, 2016

Dissertation completed October 12, 2016

Iris recognition is a promising biometric surveillance technology. However, the inability of an iris camera to operate across a large range severely restricts its use. For example, subjects are required to either stand still at a fixed standoff distance or move slowly through a pre-defined and narrow zone during the capture. Such restrictions pose sever challenges for scaling iris recognition systems that can be used with multiple subjects and in crowded areas.

Two main methods for improving the imaging volume of current iris cameras have been proposed recently: By making the imaging system's response insensitive to focusing errors using wavefront coding. Or by aggregating a large imaging volume using multiple cameras juxtaposed in time or space. While the wavefront coding systems improve the imaging volume by a few folds at close standoff distances, they generally entail high computational cost and are plagued by low SNR. The second method, which requires multiple synchronized cameras for tracking and capturing subjects with the specified volume, has significant system complexity and incur high system cost.

To extend the imaging volume of iris acquisition systems by multiple folds while using a single camera, I propose to use a combination of classical scheimpflug photography with modern computational imaging. Using scheimpflug imaging techniques, the plane of sharp focus and the associated DOF can be oriented within a prescribed imaging volume. An optimal orientation of the DOF will be found that maximizes the ability to capture in-focus iris images from multiple subjects positioned within the volume. Computational imaging techniques will be used to address the space variance associated with scheimpflug imaging, and for further improving the spatial resolution of the camera.

The complexity of such a system is minimal as it will not require multiple cameras and sophisticated tracking mechanism. This system can be scaled simply by using a lens with higher magnification and/ or a sensor with larger area which can be highly cost effective and efficient for installment in public places.

TABLE OF CONTENTS

LIST OF FIGURES

Figure

LIST OF TABLES

Tables

DEDICATION

Dedicated to my wife, parents, parents-in-law, brother, sister, and friends.

Chapter 3

MODEL OF SCHEIMPFLUG IMAGING – I: PROPERTIES OF IMAGE

Essentially, all models are wrong, but some are useful.

—George Box

For our investigation of the use of a Scheimpflug camera for extending the imaging volume of iris cameras, we require a model that includes the essential characteristics of Scheimpflug imaging. Although there are existing models, several of them use the thin lens approximation that are inaccurate. For example, it is impossible to accurately describe the shift in the image field due to lens rotation using a thin lens model. Further, models that do use thick-lens abstraction, while accurate, do not explicitly consider the effects of the pupils (defined later) on image formation. The lack of pupil parameters in these models makes it hard to predict the geometric properties of the image obtained using a Scheimpflug camera in which the lens and image planes are free to rotate about independent pivots. Therefore, we develop a new model that depicts the explicit dependence of the pupils on the properties of the image in Scheimpflug cameras. We have broken down the modeling process into two chapters—in Chapter 3 (this chapter) we develop the relationship between a world point and its image in a Scheimpflug camera, verify the model using optical ray tracing in Zemax, and finally study the consequence of rotating the sensor and lens on

the geometric properties of the image using our model. In Chapter 4 we derive equations that relates the angles and directed distances between the object, lens and sensor when the object plane is in focus.

Conventional imaging systems consists of a lens and an *image plane* on which a sharp image of an *object plane* is formed. The object and image planes are called *conjugates*. Further, amongst the several possible planes that are perpendicular to the optical axis and pass through the lens, we designate the one as the *lens plane* that provides some advantage in the geometric model. For example, the plane through the lens center and the plane through the object-side principal point are designated as the lens planes in the thin-lens and thick-lens models respectively. In our model, the lens plane is the plane through the center of the entrance pupil (defined later).

The plane in the object space that is in sharp focus is called the Plane of Sharp Focus (PoSF). In the *fronto-parallel* configuration used in most camera designs, the lens and the sensor planes are parallel to each other and perpendicular to the optical axis. In such designs, the physics of optical imaging—described by the *Gaussian Formula*—dictates that the Plane of Sharp Focus must be parallel to the lens and image planes. In contrast, the lens and image planes in a Scheimpflug camera are free to swivel about their pivots (as shown in Figure 3.1) resulting in a corresponding swivel of the PoSF. We exploit this feature—the freedom to arbitrarily orient the PoSF—of Scheimpflug imaging to improve the depth of field of the iris acquisition devices. However, the degrees of freedom offered by the Scheimpflug camera comes at the cost of added complexity of operation. Therefore, a rich description of such cameras requires the development of a general model. In this chapter, we initiate the development of such a model of Scheimpflug imaging starting from the axioms of *geometric optics* (*ray optics*).

Assumptions are crucial and necessary for modeling that enable its expediency but limits its applicability. For the model described herein, we assume paraxial imaging, rotational symmetry

and aberration-free optics in order to make the problem tractable. Additionally, we assume the refractive index of the lens elements and the interstitial medium to be isotropic (uniform along all directions) and homogeneous (uniform at all positions); this assumption imposes rectilinear propagation of light. Further, we assume the lens is surrounded by air (of refractive index equal to one). Consequently, the front and back focal lengths are equal, and the two nodal points coincide with the corresponding principal points.

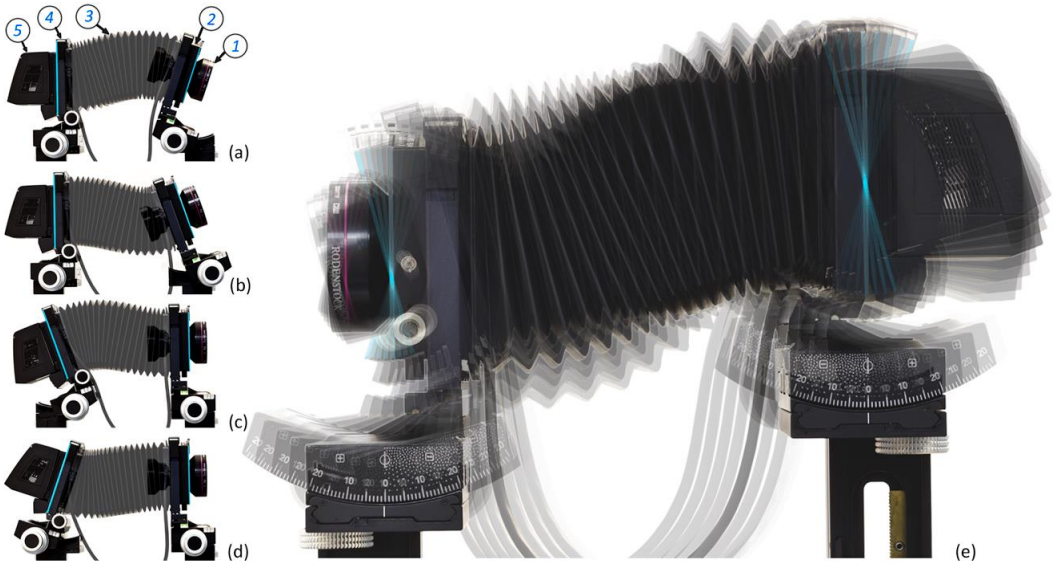

Figure 3.1 Scheimpflug camera movements. Insets (a), (b), (c), and (d) depict key camera movements—lens and sensor plane tilts about a horizontal axis—amongst several possible, in a Sinar P3 camera. Labels indicate the lens (1), the lens standard (2), bellows (3), sensor standard (4), and the sensor (5). The cyan lines on the two standards accentuates the orientations. Inset (e) is a superimposed sequence of images of the camera with the two standards in a multitude of orientations. The physical locations of the two pivots emerge at the intersection of the superimposed cyan lines.

In the following sections of this chapter we derive a general geometric imaging model that allow the both the sensor and a thick lens to be oriented arbitrarily about their own pivots, and directly incorporate important pupil related parameters in the model. We then verify the accuracy of the model using ray-tracing in Zemax. Following the verification, we study the consequences of

the model and note some of the important predictions that will ultimately allow us to build an extended depth-of-field imaging system.

3.1 Introduction

Optical imaging systems consist of several groups of elements; those elements endowed with optical power bends rays of light. The tiniest orifice in the system is called the *system aperture* or *stop*. Its interaction with the elements in the system gives rise to the pupils.

Pupils are the sine qua non of optical systems. They are indispensable in the design and specification of all optical systems, in both domains of *ray* and *wave optics*. The *entrance pupil* (E) is the image of the stop seen through the elements preceding it is. The *exit pupil* ($\acute{E}$) is the image of the stop seen through the elements following it is. The region preceding the entrance pupil, which includes the objects and light sources, is called the object space; and the region following the exit pupil, which includes the image plane, is called the image space. The size and position of the stop (and hence the pupils) affect image resolution, aberration, brightness, and geometry.

Rotationally symmetric lenses have an axis of symmetry—the optical axis. A ray coincident with the optical axis traverses undeviated through the lens. Planes passing through the axis of such lenses are the meridional planes. Rays restricted to the meridional planes are *meridional rays*. Patterns formed by the meridional rays on either side of the optical axis are mirror-reversed, exhibiting bilateral symmetry. Figure 3.2 shows two types of meridional rays, traced in Zemax, that are fundamental to geometric analysis [1,2]. The *marginal ray* (MR) originates from the axial object position and skirts the edges of the aperture and pupils (virtually); the *chief ray* (CR) starts

at an off-axis object point and pierces the centers of the aperture and pupils[1] (virtually). This pair of rays determines the location and size of the pupils, the position of the image, and the magnification. Furthermore, the bundle of chief rays from the object space converge at the center of the entrance pupil—thus *homocentric*—forming the vertex of the object-space perspective cone; in the image space, the bundle of chief rays diverges from the center of the exit pupil producing the vertex of the image-space perspective cone.

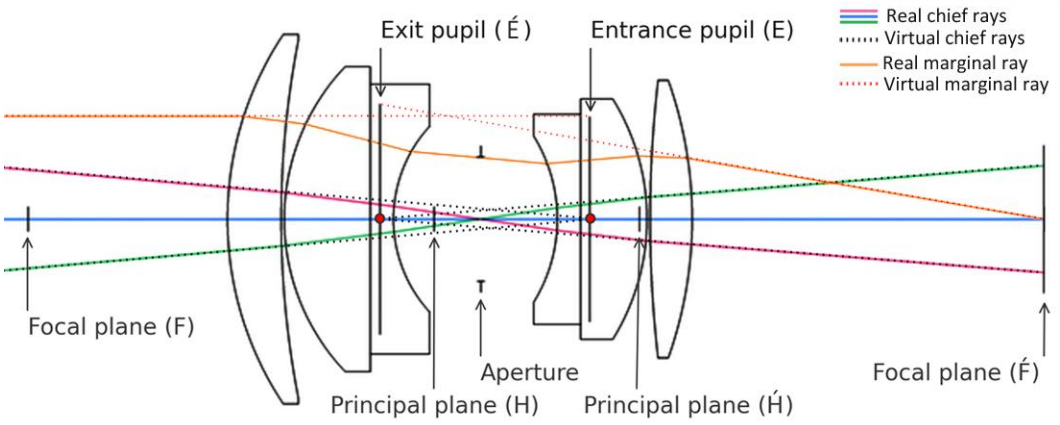

Figure 3.2 Fundamental rays (in the meridional plane) and pupils in a Double Gauss lens for an object at infinity. The chief rays—close to the optical axis (0°, ±5° in the object space at entrance pupil)—appear to converge at the center of entrance pupil and diverge from the center of exit pupil. The marginal ray, parallel to the optical axis since the object is at infinity, appear to skirt the edges of the two pupils. The red circles specify the vertices of the perspective cones (centers of the pupils). The rays were traced in Zemax.

Imagine a film projector working backwards. Imagine the stream of light rays flowing from the illuminated portion of the scene towards a small circular hole in the projector. This pencil of rays forms a conical volume of light—the perspective cone—with its vertex at the hole and its base towards the scene. The "illuminated portion" is the angular extent of the scene visible in the image,

[1] In the presence of spherical aberrations, the chief ray goes through the center of the aperture but may not exactly go through the center of the pupils [2,3].

confined by the circumferential chief rays. These extreme chief rays determine the opening angle of the cone. The "small hole" represents the entrance pupil of a camera or the pupil at the center of the iris in an eye. In the image space (behind the hole), the ray-pencil form another cone with the vertex at the center of the exit pupil. This image-space perspective cone projects the light from the scene onto the film surface or the retina in the eye. This process of image formation, known as the *central projection*, is fundamental to all imaging systems—inanimate and animate—including the camera and the eye. While the opening angle of the object-space perspective cone determines the field-of-view, its counterpart in the image space determines the angular dimension of the image. The ratio of the pupil sizes (pupil magnification) determines the relationship between the image and object-space opening angles of the two perspective cones [4,5].

3.2 Notations

- *Coordinate system*: Right-handed, with the positive z-axis oriented along the direction of light travel (left to right in the plane of drawing).
- *Scalars*: written as small letters (e.g. x). *Vectors*: small bold letters (e.g. $\mathbf{x}$). *Matrices*: written as capital letters (e.g. M).
- *Object and image space*: Non-primed quantities represent object space (e.g. x, $\mathbf{x}$). Primed quantities represent image space (e.g. $\acute{x}$, $\acute{\mathbf{x}}$).
- *Unit vectors*: represented using a hat (ˆ). The only exception is the direction cosine vectors which have unit norm, but are represented without the top hat (e.g. $\boldsymbol{l}$).
- *Reference frames*: Coordinate reference frames are denoted using curly brackets (e.g. $\{C\}$ represents the camera coordinate frame).
    - A left superscript on a variable indicates the frame of reference. For example, ${}^{O}K$ indicates that the variable K is expressed respect to the world coordinate frame $\{O\}$. If no reference is explicitly stated, then variable is expressed with

respect to the world coordinate frame (or the camera coordinate frame $\{C\}$ if the camera coordinate frame and the world coordinate frame are the same).

- A subscript is used to associate a variable with a specific optical parameter. For example, the subscript e in variable d_e is used to represent the location of the entrance pupil, and the subscript ℓ in ${}^{C}R_{\ell}$ is used to represent the rotation matrix applied to the lens plane in the camera frame $\{C\}$, etc. If the camera coordinate frame is the same as the world coordinate frame, then the notation R_{ℓ} shall be used (the superscript is dropped for convenience).
- Indices into matrices and vectors start from one (1). For example, $\hat{\boldsymbol{n}}(3)$ is the third element of the unit normal vector $\hat{\boldsymbol{n}}$, and $R_{\ell}(1,2)$ is the element in the first row and second column of the matrix R_{ℓ}. Further, a $m \times n$ matrix R_{ℓ} is represented in terms of its columns as $R_{\ell} = [\boldsymbol{r}_{\ell,1} \quad \boldsymbol{r}_{\ell,2} \quad \cdots \quad \boldsymbol{r}_{\ell,n}]$, where $\boldsymbol{r}_{\ell,i}$ for $i = 1 \ldots n$ are the n columns of R_{ℓ}.

3.3 Relation between pupil magnification and chief ray angle

The *pupil magnification* m_p is defined as the ratio of the paraxial exit-pupil diameter to the entrance-pupil diameter [4,6,7].

Figure 3.3 illustrates the meridional and sagittal planes associated with an arbitrarily located object of height y above the optical axis and its image of height $\acute{y}$ in a typical optical system. The figure also shows the chief ray from the object's edge further from the optical axis, the marginal ray from the axial point in the object, and the two pupils contained in the meridional plane. The schematic, although simple, is quite general as a (meridional) plane always exist for a given object point irrespective of its position in the three-dimensional space, if the lens is rotationally symmetric.

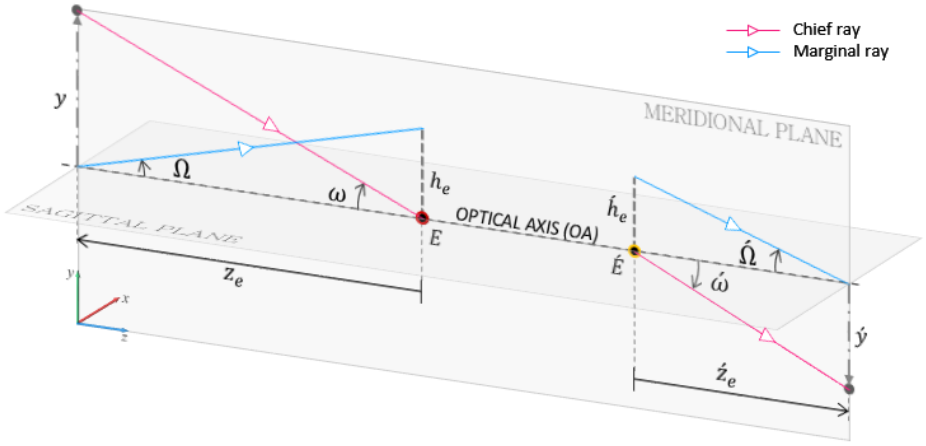

Figure 3.3 Schematic of chief and marginal rays. The ratio of the tangents of the chief ray angles in the object space to the image space yields the pupil magnification.

Let the angles between the chief ray and the optical axis (called the *ray-angle*) in the object and image space be ω and $\acute{\omega}$ respectively. Also, let the angles produced by the marginal ray with the optical axis in the object and image space be Ω and $\acute{\Omega}$ respectively. Then, we can obtain the relation between the chief-ray ray-angles—ω and $\acute{\omega}$—and the pupil magnification m_p as follows:

From the Figure 3.3 we obtain,

$$\tan(\Omega) = \frac{h_e}{z_e}, \qquad \tan(\omega) = \frac{y}{z_e},$$
$$\tan(\acute{\Omega}) = \frac{\acute{h}_e}{\acute{z}_e}, \qquad \tan(\acute{\omega}) = \frac{\acute{y}}{\acute{z}_e}. \tag{3.1}$$

Eliminating z_e and $\acute{z}_e$ after dividing $\tan(\acute{\omega})$ by $\tan(\omega)$, we have

$$\frac{\tan(\omega)}{\tan(\acute{\omega})} = \frac{\acute{h}_e}{h_e}\frac{y\tan(\Omega)}{\acute{y}\tan(\acute{\Omega})} \approx \frac{\acute{h}_e}{h_e}\frac{y\,\Omega}{\acute{y}\,\acute{\Omega}}. \tag{3.2}$$

A common observation in imaging is that we can increase the transverse magnification ($\acute{y}/y$) by increasing the lens-to-image-plane distance while correspondingly decreasing the lens-to-object-plane distance in order to maintain focus on the object. However, increasing (decreasing)

the image plane distance proportionally decreases (increases) the marginal ray angle $\acute{\Omega}$ (see Figure 3.3). Consequently, the angular magnification ($\acute{\Omega}/\Omega$) decreases with increase in lens-to-image-plane distance. Therefore, a large transverse magnification is associated with a correspondingly small angular magnification. This result follows from a more general theory called the *Lagrange invariant* property [4] of the two rays (the chief ray and the marginal ray) when applied between conjugate locations. As per the invariant property, the product of the transverse magnification and the angular magnification equals to one, i.e., $\left(\frac{\acute{y}}{y}\right)\left(\frac{\acute{\Omega}}{\Omega}\right) = 1$ or $y\Omega = \acute{y}\acute{\Omega}$. Cancelling the corresponding terms in Eq. (3.2) yields the relationship between the pupil magnification and the object and image space chief ray angles as:

$$\boxed{\frac{\tan(\omega)}{\tan(\acute{\omega})} = m_p} \tag{3.3}$$

where,

m_p	Pupil magnification.
ω	Angle that the chief ray makes with the optical axis in the object (input) space.
$\acute{\omega}$	Angle that the chief ray makes with the optical axis in the image (output) space.

The above relation (Eq. (3.3)) has been previously derived in [7] using a different formulation.

For a given optical system with fixed focal length, the pupil magnification m_p is constant. This constancy of the ratio of the tangents of the chief ray angles for varying object (and image) heights is a necessary and sufficient condition for distortion-free imaging known as the *Airy's Tangent-Condition* [3,7]. Eq. (3.3) also suggests that when $m_p = 1$ the perspective cones in the

object- and image-space are symmetric. In the following section, we will use Eq. (3.3) to derive the relationship between the direction cosines of the object-space (input) chief rays and direction cosines of the image-space (output) chief rays.

3.4 Transfer of chief ray's direction cosines between the pupils

The direction cosines, a unit vector of cardinality three, specify the direction of a ray. Its elements are the cosines of the angles the ray makes with the three coordinate axes. In other words, the elements of the direction cosine vector are the projections of the unit vector in the direction of the ray on the x-, y-, and z-axes. In the absence of aberrations, the chief ray starts from an object point, passing through the center of the entrance pupil (virtually), the aperture stop, exit pupil (virtually), and ends at the image point. Suppose we know the direction cosine of the chief ray in the object space (between the object point and the entrance pupil), what is the direction cosine of the chief ray in the image space (between the exit pupil and image point)? Furthermore, what is the relation between the input and output chief ray's direction cosines if the lens is swiveled about a pivot point along the optical axis?

We begin by solving a specific problem of the *transfer* of the direction cosines between the pupils in which the optical axis coincides with the z-axis of the camera frame $\{C\}$. The configuration of this specific problem is show in Figure 3.4. Subsequently, we will deduce the general *transfer* expression in which the optical axis is free to swivel about the origin of $\{C\}$. Let $\boldsymbol{l} = [l, m, n]^T$ be the direction cosine of the chief ray from an object point **x** to the center of the entrance pupil, and let $\acute{\boldsymbol{l}} = \left[\acute{l}, \acute{m}, \acute{n}\right]^T$ be the corresponding direction cosine of the chief ray from the exit pupil to the image point. The parameters **x**, $\boldsymbol{l}$, and $\acute{\boldsymbol{l}}$ are specified with respect to frame $\{C\}$.

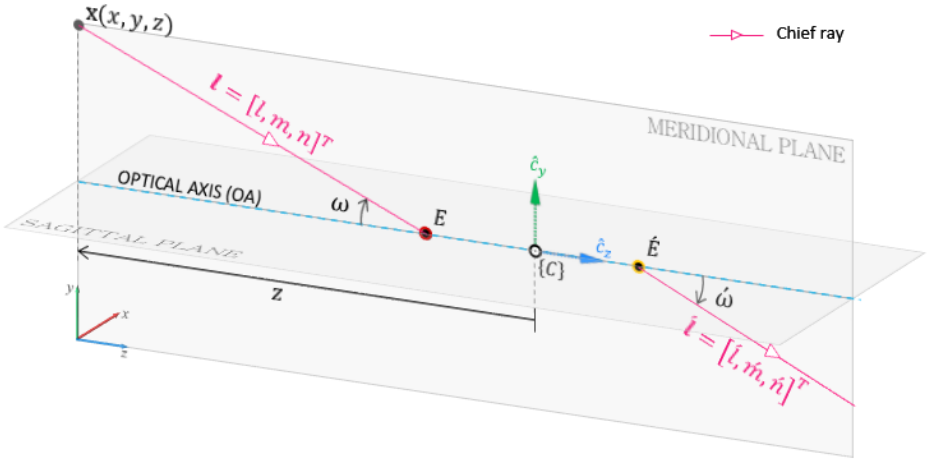

Figure 3.4 Specific problem—optical axis coincides with reference frame's z-axis. If θ and $\acute{\theta}$ are the angles of the chief ray with the optical axis in the object and image space respectively, then $\omega = \theta = \cos^{-1}(n)$ and $\acute{\omega} = \acute{\theta} = \cos^{-1}(\acute{n})$.

If θ and ϕ are the zenith and azimuthal angles of the chief ray in the object space, and $\acute{\theta}$ and $\acute{\phi}$ the corresponding angles in the image space, then the direction cosines, in $\{C\}$, are:

$$\begin{aligned} l &= \cos(\phi)\sin(\theta) & \acute{l} &= \cos(\acute{\phi})\sin(\acute{\theta}) \\ m &= \sin(\phi)\sin(\theta) & \acute{m} &= \sin(\acute{\phi})\sin(\acute{\theta}) \\ n &= \cos(\theta) & \acute{n} &= \cos(\acute{\theta}) \end{aligned} \tag{3.4}$$

Since the optical axis is aligned with the z-axis, we have $\omega = \theta$ and $\acute{\omega} = \acute{\theta}$. Substituting the expressions for $\sin(\theta)$, $\cos(\theta)$, $\sin(\acute{\theta})$ and $\cos(\acute{\theta})$ from Eq. (3.4) into Eq. (3.3) we obtain:

$$\begin{gathered} \frac{l}{\acute{l}}\frac{n}{\acute{n}}\cos(\acute{\phi}) = m_p\cos(\phi) \\ \text{and} \\ \frac{m}{\acute{m}}\frac{n}{\acute{n}}\sin(\acute{\phi}) = m_p\sin(\phi) \end{gathered} \tag{3.5}$$

Further, since the input and out chief rays are confined to the same meridional plane [1,2], $\acute{\phi} = \phi$, yielding $\acute{l}$ and $\acute{m}$ in terms of l and m, the ratios of $\acute{n}$ to n, and m_p:

$$\acute{l} = \frac{1}{m_p}\frac{\acute{n}}{n}\, l \ ,$$
$$\text{and} \tag{3.6}$$
$$\acute{m} = \frac{1}{m_p}\frac{\acute{n}}{n}\, m \ .$$

From (3.3) we have

$$m_p \ = \ \frac{\tan(\theta)}{\tan(\acute{\theta})} \ = \ \frac{\sin(\theta)\cos(\acute{\theta})}{\sin(\acute{\theta})\cos(\theta)} \ = \ \sqrt{\frac{1-n^2}{1-\acute{n}^2}} \times \frac{\acute{n}}{n} \ , \tag{3.7}$$

which after simplification yields $\acute{n}$ in terms of the pupil magnification m_p and input n as

$$\acute{n} = \pm \frac{m_p}{\sqrt{1+\left(m_p^2-1\right)n^2}} n \ . \tag{3.8}$$

Combining Eqs. (3.6) and (3.8), we obtain the expression for output direction cosine of the chief ray in terms of its input direction cosines and the pupil magnification as:

$$\begin{bmatrix} \acute{l} \\ \acute{m} \\ \acute{n} \end{bmatrix} = \pm \frac{1}{\sqrt{1+\left(m_p^2-1\right)n^2}} \begin{bmatrix} 1 & 0 & 0 \\ 0 & 1 & 0 \\ 0 & 0 & m_p \end{bmatrix} \begin{bmatrix} l \\ m \\ n \end{bmatrix} \ , \tag{3.9}$$

which we can write compactly as:

$$\acute{\boldsymbol{l}} = \frac{1}{\sqrt{1+\left(m_p^2-1\right)n^2}} M_p \boldsymbol{l} \ . \tag{3.10}$$

Our objective is to derive the expression for the transfer of the chief ray's direction cosines from entrance pupil to exit pupil for arbitrary orientation of the optical axis as shown in Figure 3.5. Although a formal derivation is provided in Appendix A.1, we can readily infer the general

expression for the *transfer* from Eq. (3.10). Suppose we swivel the optical axis about the origin of the camera frame $\{C\}$. This rotation can be described by the matrix $R_\ell \in \mathbb{R}^{3\times3}$. As before, we designate the ray from the object point **x** to the (new position of the) center of the entrance pupil as the chief ray. Let us also suppose that we have another coordinate frame, $\{\mathcal{L}\}$, sharing its origin with $\{C\}$ and its z-axis coincident with the optical axis. If $\boldsymbol{l}$ be the direction cosine of the chief ray from the object point in the frame $\{C\}$, then the direction cosine in the frame $\{\mathcal{L}\}$ is ${R_\ell}^T \boldsymbol{l}$ and the third element of the direction cosine is $\boldsymbol{r}_{\ell,3}^T \boldsymbol{l}$, where $\boldsymbol{r}_{\ell,3}$ is the third column of R_ℓ. Representing $n_R = \boldsymbol{r}_{\ell,3}^T \boldsymbol{l}$, the direction cosine of the chief ray emerging from the exit pupil is obtained by substituting $\boldsymbol{r}_{\ell,3}^T \boldsymbol{l}$ for $\boldsymbol{l}$ and n_R for n in Eq. (3.10):

$$\acute{\boldsymbol{l}} = \pm \frac{1}{\sqrt{1 + \left(m_p^2 - 1\right) n_R^2}} M_p R_\ell^T \boldsymbol{l}$$

The above expression represents the output direction cosine in the coordinate frame $\{\mathcal{L}\}$. In order to transform the output direction cosine from the coordinate frame $\{\mathcal{L}\}$ to the camera frame $\{C\}$ we need to multiply the direction cosine vector by R_ℓ to obtain:

$$\acute{\boldsymbol{l}} = \pm \frac{1}{\sqrt{1 + \left(m_p^2 - 1\right) n_R^2}} R_\ell M_p R_\ell^T \boldsymbol{l} \tag{3.11}$$

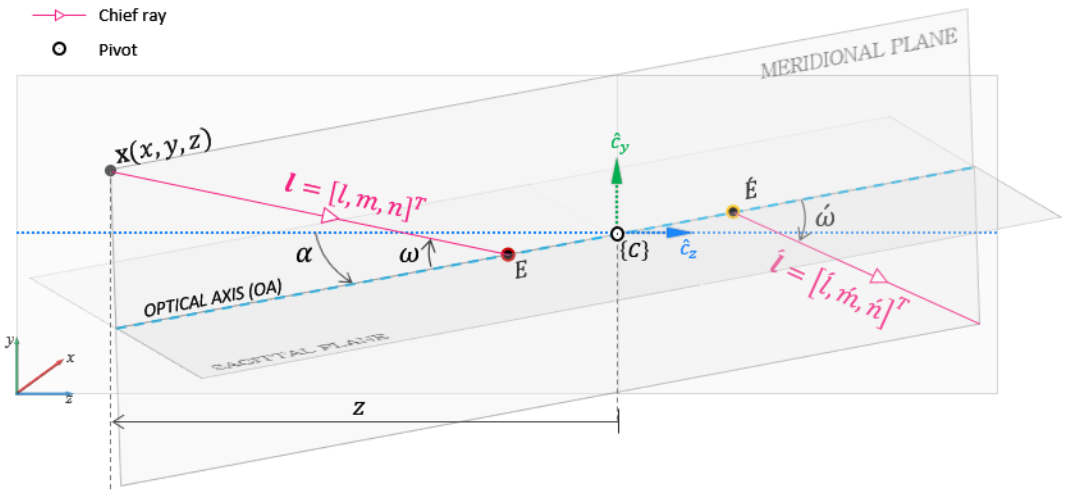

Figure 3.5 Configuration of the general problem—optical axis pivots freely about the origin of $\{C\}$.

The positive or negative sign of the direction cosine determines the forward or backward direction of light-travel along a rectilinear path. Under the assumptions of isotropy and homogeneity, the only condition under which a ray of light emerges in an antipodal path from an interface is if it encounters a mirror surface *normally*. This condition does not arise within the context of our problem. Therefore, without any loss of generality, we can drop the negative sign in Eq. (3.11); accordingly, the output direction cosines assume the sign of the corresponding input direction cosines. Therefore, we obtain the general expression for the direction cosines of the chief ray in the image space as:

$$\boxed{\acute{\boldsymbol{l}} = \frac{1}{\sqrt{1 + \left(m_p^2 - 1\right) n_R^2}} R_\ell M_p R_\ell^T \boldsymbol{l}} \tag{3.12}$$

where,

n_R	The third element of the input direction cosine vector following rotation. $n_R = \boldsymbol{r}_{\ell,3}^T \boldsymbol{l}$
$\boldsymbol{l}$	Input or object space chief ray's direction cosine vector from the object point **x** to the entrance pupil.
$\acute{\boldsymbol{l}}$	Output or image space chief ray's direction cosine vector emerging from the exit pupil.
M_p	Equal to $diag(1, 1, m_p)$, where m_p is the pupil magnification.
R_ℓ	Rotation matrix used to describe the orientation of the lens plane.
$\boldsymbol{r}_{\ell,3}$	The third column of R_ℓ.

Note that Eq. (3.12) only describes the output chief ray's direction cosines—a free vector. The exact output chief ray is obtained from the knowledge of the direction cosine and the location of the exit pupil in the appropriate reference frame.

Although it is not obvious from the expression Eq. (3.12), we expect $\acute{\boldsymbol{l}}$ to have unit magnitude. We present a proof in Appendix A.2 that shows the ℓ^2-Norm (magnitude) of $\acute{\boldsymbol{l}}$ is indeed equal to one, and $\{1 + (m_p^2 - 1)n_R^2\}^{-1/2}$ is the normalizing term.

Furthermore, we can draw the following inferences about $\acute{\boldsymbol{l}}$ from the Eq. (3.12):

1. If the pupil magnification, $m_p = 1$, then $\acute{\boldsymbol{l}} = \boldsymbol{l}$, which implies that the opening angles of the image and object space perspective cones are equal, irrespective of the orientation of the optical axis. Then, the lens is symmetric about a plane perpendicular to the optical axis (in addition to the rotational symmetry about the optical axis). It must not come as a surprise that symmetric lenses are can be reversed without affecting any optical system properties [6].
2. If we let $Q = R_\ell$, such that $A = QM_pQ^T$, then we can write $\acute{\boldsymbol{l}} \cong kA\boldsymbol{l}$, where k is the scalar normalization term. Furthermore, as M_p is a diagonal matrix, and Q is orthonormal, we

can immediately recognize the form $A = QM_pQ^T$ as the Eigen value decomposition of a symmetric matrix A, with $\boldsymbol{q}_i = \boldsymbol{r}_{\ell,i}$ for $i = 1,2,3$—the columns of Q—as the eigenvectors and $\lambda = \{1, 1, m_p\}$ the corresponding eigenvalues. i.e., as M_p is a diagonal matrix,

$$\begin{aligned} A &= QM_pQ^T \\ &= \sum_{i=1}^{3} M_p(i,i)\boldsymbol{q}_i\boldsymbol{q}_i^T \ , \end{aligned}$$

and

$$\begin{aligned} \acute{\boldsymbol{l}} &= k\sum_{i=1}^{3} M_p(i,i)\boldsymbol{q}_i\boldsymbol{q}_i^T\boldsymbol{l} \\ &= k(\boldsymbol{q}_1^T\boldsymbol{l})\boldsymbol{q}_1 + k(\boldsymbol{q}_2^T\boldsymbol{l})\boldsymbol{q}_2 + k\, m_p(\boldsymbol{q}_3^T\boldsymbol{l})\boldsymbol{q}_3 \ . \end{aligned} \tag{3.13}$$

In Eq. (3.13) the terms $\left(\boldsymbol{q}_i^T\boldsymbol{l}\right)$ for $i = 1, 2, 3$ are the projections of the input direction cosine along the eigenvectors $\boldsymbol{q}_i = \boldsymbol{r}_{\ell,i}$. Also, $\boldsymbol{q}_3 = \boldsymbol{r}_{\ell,3}$, the third column of the rotation matrix R_ℓ, is the direction of the optical axis.

3.5 Image formation for arbitrary orientation of the lens and image plane

Geometric imaging is a mapping (*bijective* in projective space) between points in the three-dimensional world space to corresponding points on a mathematical surface that we call the *image*. Here we aim to study the nature of this mapping on a planar surface—the image plane—for arbitrary orientations of the lens and image planes. To that effect, we will use the knowledge of the transfer of direction cosines of the chief ray derived previously.

An extended object emanates a multitude of chief rays that reach the image space through the lens elements and the stop. The locus of points formed by the intersection of these rays with the image plane constitutes the *projection* of the object in the image plane [8,9]. Further, we generally identify the projection of the object point as an "image" when the pencil of rays from the object point geometrically converge at a single point in the image space.

For simplicity, we assume that the lens is unencumbered by radial distortions and optical aberrations. Figure 3.6 represents a schematic of the problem in which we have introduced an image plane whose orientation is described by its surface normal $\hat{\boldsymbol{n}}_i$. Two local frames are also introduced: the frame $\{P\}$ is attached to the optical axis with its origin at entrance pupil, and the frame $\{I\}$ attached to the image plane with its origin at the image plane pivot. The image plane is free to tilt or swing about its local x-axis or y-axis respectively at the image plane pivot.

Let the exit pupil ($\acute{E}$) be located $\acute{d}_e$ units from the pivot point along the optical axis. Following the rotation of the optical axis, by applying the matrix $R_\ell \in \mathbb{R}^{3\times3}$, the position of the exit pupil in camera frame $\{C\}$ is given as $R_\ell\left[0,0,\acute{d}_e\right]^T = \acute{d}_e \boldsymbol{r}_{\ell,3}$.

We can represent the chief ray emerging from the exit pupil with direction cosine $\acute{\boldsymbol{l}}$ by the parametric equation:

$$\acute{\mathbf{x}}(\lambda) = \acute{d}_e\, \boldsymbol{r}_{\ell,3} + \frac{\lambda}{\sqrt{1+\left(m_p^2-1\right)n_R^2}}\, R_\ell M_p R_\ell^T \acute{\boldsymbol{l}}\,, \tag{3.14}$$

where $\acute{\mathbf{x}}(\lambda)$ represent points along the output chief ray in $\{C\}$. The first term on the right hand side of Eq. (3.14) is the initial position of the ray (at the center of $\acute{E}$) and λ is a real number that determines the length of the ray.

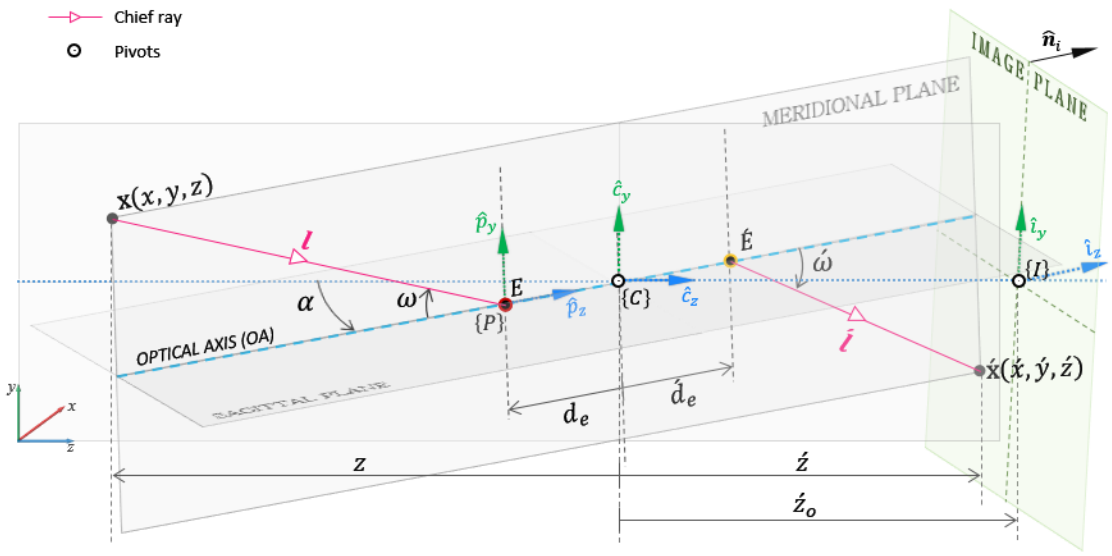

Figure 3.6 Schematic of geometric image formation. $\acute{\mathbf{x}}$ is the *central projection* of the object point **x** on image plane. The optical axis and image plane are free to swivel about the origins of coordinate frames $\{C\}$ and $\{I\}$ respectively.

We write the equation of the image plane in Hessian normal form as:

$$\hat{\boldsymbol{n}}_i^T \boldsymbol{\xi} = \acute{z}_{o\perp} \,, \tag{3.15}$$

where $\hat{\boldsymbol{n}}_i$ is the unit normal to the image plane, $\acute{z}_{o\perp}$ is the perpendicular distance of the plane from the origin of frame $\{C\}$, and $\boldsymbol{\xi}$ is a point on the image plane.

We obtain the expression for λ (in Eq. (3.14)) for which the ray intersects the image plane by equating $\boldsymbol{\xi}$ to $\acute{\mathbf{x}}$, multiplying Eq. (3.14) by $\hat{\boldsymbol{n}}_i^T$, and rearranging the terms:

$$\underbrace{\hat{\boldsymbol{n}}_i^T \acute{\mathbf{x}}}_{\acute{z}_{o\perp}} = \acute{d}_e \hat{\boldsymbol{n}}_i^T \boldsymbol{r}_{\ell,3} \; + \frac{\lambda}{\sqrt{1 + \left(m_p^2 - 1\right) n_R^2}} \hat{\boldsymbol{n}}_i^T \, R_\ell M_p R_\ell^T \boldsymbol{l} \,,$$

$$\lambda = \frac{\left(\acute{z}_{o\perp} - \acute{d}_e \hat{\boldsymbol{n}}_i^T \, \boldsymbol{r}_{\ell,3}\right) \sqrt{1 + \left(m_p^2 - 1\right) n_R^2}}{\hat{\boldsymbol{n}}_i^T \, R_\ell M_p R_\ell^T \boldsymbol{l}} \,. \tag{3.16}$$

Substituting Eq. (3.16) into Eq. (3.14) we get

$$\acute{\mathbf{x}} = \acute{d}_e \, \boldsymbol{r}_{\ell,3} + \frac{\left(\acute{z}_{o\perp} - \acute{d}_e \widehat{\boldsymbol{n}}_i^T \, \boldsymbol{r}_{\ell,3}\right)}{\widehat{\boldsymbol{n}}_i^T \, R_\ell M_p R_\ell^T \boldsymbol{l}} \, R_\ell M_p R_\ell^T \boldsymbol{l} \tag{3.17}$$

Now we proceed to find the expression for the perpendicular distance $\acute{z}_{o\perp}$ in terms of the known parameters. The origin of the image plane's local reference frame, $\{I\}$, is located at the intersection of the z-axis of camera frame $\{C\}$ with the image plane (see Figure 3.7). Given the location of the image plane's pivot, $(0,0,\acute{z}_o)$, we can describe the orientation of the image plane using the surface normal. The image plane's surface normal is obtained by applying the rotation matrix R_i to the unit vector $[0,0,1]^T$:

$$\widehat{\boldsymbol{n}}_i = R_i \begin{bmatrix} 0 \\ 0 \\ 1 \end{bmatrix}. \tag{3.18}$$

The equation of the image plane as represented by Eq. (3.15) is

$$\widehat{\boldsymbol{n}}_i^T \boldsymbol{\xi} = \acute{z}_{o\perp} \, .$$

Since $\boldsymbol{\xi} = [0, 0, \acute{z}_o]^T$ is a point on the plane, we obtain $\acute{z}_{o\perp}$ as:

$$\acute{z}_{o\perp} = \widehat{\boldsymbol{n}}_i^T \begin{bmatrix} 0 \\ 0 \\ \acute{z}_o \end{bmatrix} = \widehat{\boldsymbol{n}}_i(3)\acute{z}_o \, . \tag{3.19}$$

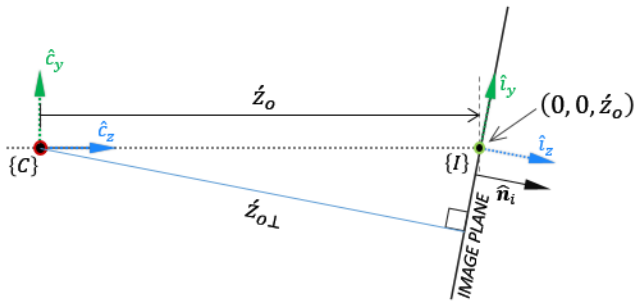

Figure 3.7 Schematic of the image plane. The image plane having surface normal $\hat{\boldsymbol{n}}_i$ is located at $\acute{z}_o$ units from the origin of camera frame $\{C\}$ along the z-axis that intersects the plane at $(0,0,\acute{z}_o)$. $\acute{z}_{o\perp}$ is the perpendicular distance from the origin to the plane. The local image coordinate frame with its origin at the intersection of the image plane and z-axis of the camera frame is represented by $\{I\}$.

Substituting $\acute{z}_{o\perp}$ from Eq. (3.19) into Eq. (3.17) yields the expression for the point of intersection of the chief ray with the image plane in terms of the input direction cosines as

$$\acute{\mathbf{x}} = \acute{d}_e\, \boldsymbol{r}_{\ell,3} + \frac{\left(\hat{\boldsymbol{n}}_i(3)\acute{z}_o - \acute{d}_e\, \hat{\boldsymbol{n}}_i^T\, \boldsymbol{r}_{\ell,3}\right)}{\hat{\boldsymbol{n}}_i^T\, R_\ell M_p R_\ell^T \boldsymbol{l}}\, R_\ell M_p R_\ell^T \boldsymbol{l}\,. \tag{3.20}$$

Let the entrance pupil be located at a distance d_e from the pivot point along the optical axis in the camera frame $\{C\}$. Then, similar to the description of the exit pupil, the location of the entrance pupil in $\{C\}$ is given as:

$$\mathbf{x}_e = R_\ell\, [0,0,d_e]^T = d_e\, \boldsymbol{r}_{\ell,3}\ . \tag{3.21}$$

Further, we express the direction cosine components in terms of the Cartesian coordinates of the object point and entrance pupil in the camera frame $\{C\}$ as:

$$
\begin{aligned}
l &= \frac{x_e - x}{\sqrt{(x_e - x)^2 + (y_e - y)^2 + (z_e - z)^2}} = \frac{d_e\, R_\ell(1,3) - x}{\|\mathbf{x}_e - \mathbf{x}\|}\ , \\
m &= \frac{y_e - y}{\sqrt{(x_e - x)^2 + (y_e - y)^2 + (z_e - z)^2}} = \frac{d_e\, R_\ell(2,3) - y}{\|\mathbf{x}_e - \mathbf{x}\|}\ , \\
n &= \frac{z_e - z}{\sqrt{(x_e - x)^2 + (y_e - y)^2 + (z_e - z)^2}} = \frac{d_e\, R_\ell(3,3) - z}{\|\mathbf{x}_e - \mathbf{x}\|}\ ,
\end{aligned}
\tag{3.22}
$$

which we write compactly as:

$$
\boldsymbol{l} = \frac{\mathbf{x} - d_e\, \boldsymbol{r}_{\ell,3}}{\|\mathbf{x}_e - \mathbf{x}\|}\ . \tag{3.23}
$$

Substituting Eqs. (3.23) and (3.21) into Eq. (3.20), we obtain a general relationship between the object point $\mathbf{x}$ and its corresponding image point $\acute{\mathbf{x}}$ as:

$$
\acute{\mathbf{x}} = \acute{d}_e\, \boldsymbol{r}_{\ell,3} + \frac{\left(\widehat{\boldsymbol{n}}_i(3)\acute{z}_o - \acute{d}_e \widehat{\boldsymbol{n}}_i^T\, \boldsymbol{r}_{\ell,3}\right)}{\widehat{\boldsymbol{n}}_i^T\, R_\ell M_p R_\ell^T \left(\mathbf{x} - d_e\, \boldsymbol{r}_{\ell,3}\right)}\, R_\ell M_p R_\ell^T \left(\mathbf{x} - d_e\, \boldsymbol{r}_{\ell,3}\right) \tag{3.24}
$$

Eq. (3.24) represents the image point $\acute{\mathbf{x}}$ in the camera frame. Once an image—a two dimensional representation of the scene—has been formed, we specify positions and dimensions in the image independent of the position and orientation of the sensor and lenses (e.g. in terms of pixels in a digital image). We can transform the image coordinates in the camera frame $\{C\}$ represented by Eq. (3.24) to the image frame $\{I\}$ by observing that the origin of $\{I\}$ is displaced from $\{C\}$ by the translation vector $\boldsymbol{t}_i = [0, 0, \acute{z}_o\ ]^T$, and the standard basis vectors of frame $\{I\}$ are rotated by $R_i \in \mathbb{R}^{3\times3}$. Consequently, a point ${}^I\acute{\mathbf{x}}$ in $\{I\}$ relative to $\{C\}$ may be expressed as (see Eq. 2.53 in [10]):

$$
{}^C\acute{\mathbf{x}} = R_i\ {}^I\acute{\mathbf{x}} + \boldsymbol{t}_i\ . \tag{3.25}
$$

Therefore, we can write the expression for the image point coordinates in the image plane's reference frame as:

$$^{I}\acute{\mathbf{x}} = R_i^T \left(^{C}\acute{\mathbf{x}} - \boldsymbol{t}_i \right) \tag{3.26}$$

Substituting $^{C}\acute{\mathbf{x}}$ from Eq. (3.24) into Eq. (3.26) we obtain the expression of the two-dimensional image point in the image frame as:

$$\boxed{^{I}\acute{\mathbf{x}} = R_i{}^T \left(\acute{d}_e \, \boldsymbol{r}_{\ell,3} - \boldsymbol{t}_i \right) + \frac{\left(\widehat{\boldsymbol{n}}_i(3)\acute{z}_o - \acute{d}_e \widehat{\boldsymbol{n}}_i^T \, \boldsymbol{r}_{\ell,3} \right)}{\widehat{\boldsymbol{n}}_i^T R_\ell M_p R_\ell^T \left(^{C}\mathbf{x} - d_e \, \boldsymbol{r}_{\ell,3} \right)} \, R_i{}^T R_\ell M_p R_\ell^T \left(^{C}\mathbf{x} - d_e \, \boldsymbol{r}_{\ell,3} \right)} \tag{3.27}$$

Where,

$^{C}\mathbf{x}$	3D Cartesian coordinates (in physical units) of the world point in camera frame $\{C\}$. In our coordinate convention, the numerical value of z-component of **x** is negative.
$^{I}\acute{\mathbf{x}}$	2D Cartesian coordinates (in physical units) of the image point in the image frame $\{I\}$. Note that Eq. (3.27) produces a 3×1 vector with the third element (i.e. the $^{I}\acute{z}$ component) identically equal to zero.
M_p	Equal to $diag(1, 1, m_p)$, where m_p is the pupil magnification.
d_e	Location of the entrance pupil from the pivot (origin of $\{C\}$) along the optical axis. This scalar quantity physical units, usually in millimeters.
$\acute{d}_e$	Location of the exit pupil from the pivot (origin of $\{C\}$) along the optical axis.
$\acute{z}_o$	Location of the image plane from the pivot (origin of $\{C\}$) along the z-axis of $\{C\}$.
R_ℓ	Rotation matrix used to describe the orientation of the lens plane.
$\boldsymbol{r}_{\ell,3}$	The third column of R_ℓ.
R_i	Rotation matrix used to describe the orientation of the image plane.
$\widehat{\boldsymbol{n}}_i$	The image plane normal. $\widehat{\boldsymbol{n}}_i(3)$ denotes the z-component of the normal.
$\boldsymbol{t}_i$	Origin of the image frame with respect to camera frame; $\boldsymbol{t}_i = [0, 0, \acute{z}_o\,]^T$.

3.6 Verification of imaging equation in Zemax

We derived Eq. (3.27), which relates a three-dimensional object point to its projection in the two-dimensional image plane of a Scheimpflug camera, analytically. Now we verify the accuracy of the relationship by comparing the numerically computed values of image points (intersection of chief ray with the image plane) using Eq. (3.27) with corresponding image points obtained by tracing chief rays from a grid of points belonging to the object plane. Figure 3.8 is a layout plot of

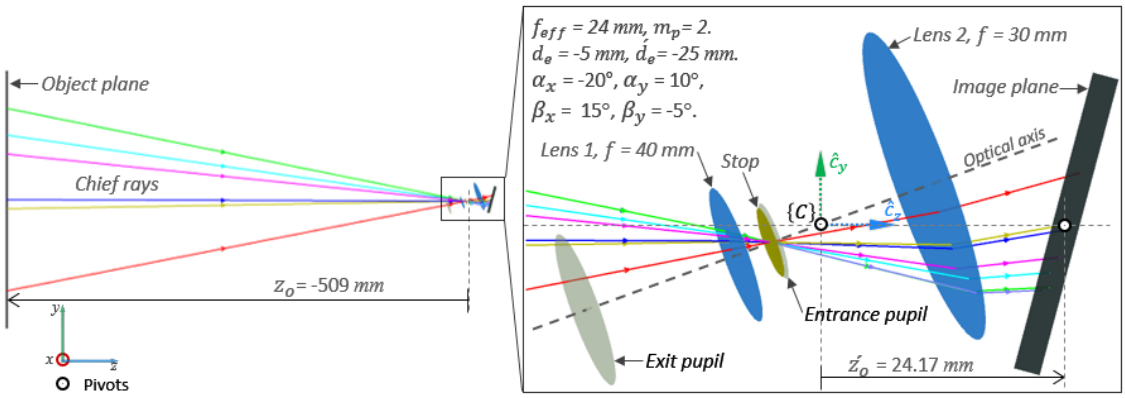

Figure 3.8 Ray tracing for verifying Eq. (3.27). Chief rays traced from a grid of points in the object plane through an ideal lens tilted about a point $d_e = -5\ mm$ away from the entrance pupil along the optical axis to the tilted image plane.

---

the optical system modeled in Zemax showing (1) an object plane, (2) an ideal lens made from two paraxial surfaces and pivoted about a point away from the entrance pupil ($d_e = -5\ mm$), and (3) an image plane pivoted about the image plane pivot along the z-axis. We can arbitrarily assign any rotation angle to both the lens and image planes (pivot at their local frame's origin) with respect to both x- and y-axis. The orientation of both planes is represented using *intrinsic* rotations matrices (composed of elemental rotations first about the x-axis followed by rotation about the new y-axis). Symbols α_x and α_y represent the angles of rotation of the lens plane about the x- and y-axes while β_x and β_y represent the angles of rotation of the image plane about the x- and y-axes. The results of the simulation are tabulated in Table 3.1, which shows the set of object points, the numerically

computed image points, the ray traced image points, and the absolute difference between the numerically computed and ray traced image points. We observe that the numerically computed and ray traced values of the image points are very close; the small difference in their values can be attributed to the error associated with floating point operations. This comparison demonstrates that the analytically derived expression (Eq. (3.27)) representing geometric relationship between a three-dimensional object point and its image point in the absence of optical aberrations is accurate.

Table 3.1 Comparison of numerically computed image points with ray traced (in Zemax) image points for the optical system shown in Figure 3.8.

World point ${}^{C}\mathbf{x}\,(x, y, z)$	Computed image point ${}^{I}\acute{\mathbf{x}}(\acute{x}, \acute{y}, \acute{z})$	Ray-traced image point ${}^{I}\acute{\mathbf{x}}_{rt}(\acute{x}, \acute{y}, \acute{z})$	Absolute difference $\left\lvert {}^{I}\acute{\mathbf{x}} - {}^{I}\acute{\mathbf{x}}_{rt} \right\rvert$
(0.0, 0.0, -509.0)	(-0.3108, -0.6291, 0.0)	(-0.3108, -0.6291, 0.0)	(1.8e-09, 3.1e-09, 7.5e-15)
(10.0, -10.0, -509.0)	(-0.8003, -0.0863, 0.0)	(-0.8003, -0.0863, 0.0)	(2.1e-09, 2.7e-09, 3.0e-15)
(-50.0, 50.0, -509.0)	(2.1291, -3.3352, 0.0)	(2.1291, -3.3352, 0.0)	(1.2e-09, 3.2e-09, 2.9e-15)
(70.71, 70.71, -509.0)	(-4.2013, -5.0221, 0.0)	(-4.2013, -5.0221, 0.0)	(2.6e-09, 5.1e-09, 4.7e-15)
(100.0, 0.0, -509.0)	(-5.5251, -1.0101, 0.0)	(-5.5251, -1.0101, 0.0)	(1.3e-09, 8.4e-09, 3.1e-15)
(0.0, 100.0, -509.0)	(-0.6031, -6.4387, 0.0)	(-0.6031, -6.4387, 0.0)	(2.2e-09, 4.0e-09, 2.2e-16)
(100.0, 100.0, -509.0)	(-5.8238, -6.8542, 0.0)	(-5.8238, -6.8542, 0.0)	(5.6e-10, 2.5e-10, 2.2e-15)

3.7 Geometric properties of images under lens and image plane rotation

Following the verification of Eq. (3.27), we use the expression to qualitatively study the effects of lens and sensor rotations on the geometric properties of the image. We also investigate the effects of pupil magnification, m_p, and location of the lens pivot on the nature of the geometric distortions. Figures 3.10 – 3.15 show the type of distortions in images—of two planes in the object space—for several lens and sensor orientations. In all these figures, the basic setup is similar to that shown in Figure 3.8 except that the object space consists of two planes—a near plane and a far

plane. The near plane is a square of 88.15 mm on each side, and the far plane is a square of 178.3 mm on each side placed at twice the distance of the near plane from the entrance pupil. The exact distance of the near plane (and consequently the far plane) from the lens vary depending upon the pupil magnification, such that the images of the two planes are 4.5 mm on each side on the sensor. Also, since the *z*-axis of the camera frame passes through the center of both object planes, the two images are coincident in the frontoparallel configuration (i.e. when the object planes are parallel to lens and image planes).

The object points consist of 7×7 square grids on each of the object planes. The corresponding "image points" are the points of intersection of the chief-rays (emanating from the object points) with the image plane (Figure 3.9 (a)). The orange "Y" markers represent the group of image points from the near object plane. The blue "inverted Y" markers represent the image points from the far object plane. Note that in frontoparallel configuration the two images of the two object planes coincide; however, for the sake of visual clarity, we separate the two set of image points horizontally by 5 *mm* on either side from the center (Figure 3.9 (b)). In Figures 3.10 – 3.15 while lighter shaded (orange and blue) markers are used to represent the points in frontoparallel configuration, darker shaded markers of either color represent the image points following the rotation of the sensor or lens. Rotation of either the lens or the sensor induces a geometric distortion of the image field in which the points across the image field translates by different amounts and

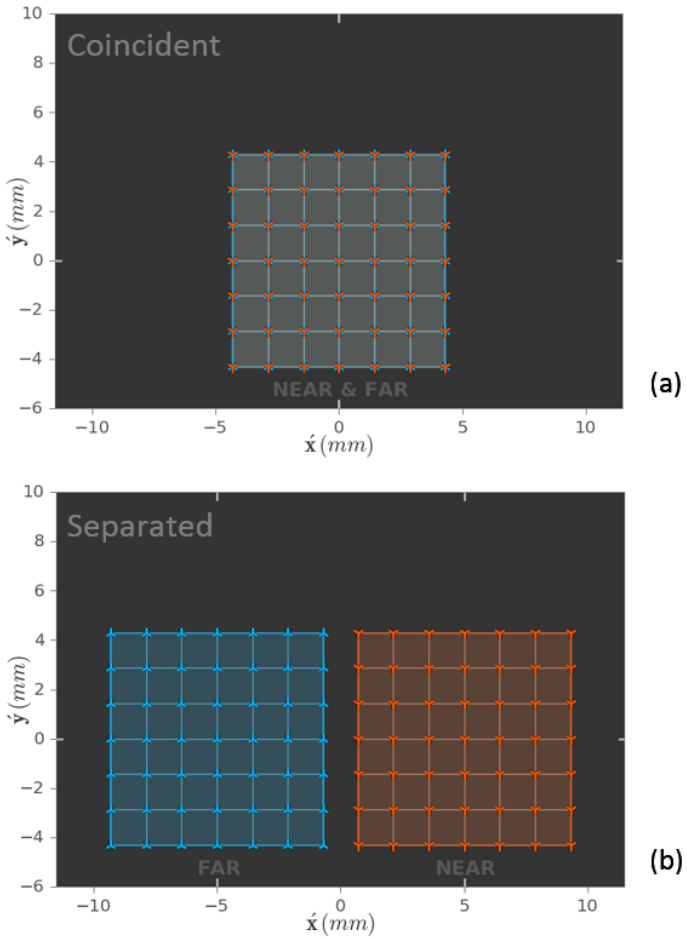

Figure 3.9 "Image points" corresponding to two object planes—a far plane twice the size of the near plane. (a) The image points are coincident. (b) The coincident image points are separated laterally for the purpose of our investigation.

---

directions. These translations are shown by the gray-to-white arrows between the original and shifted positions (drawn if the magnitude of the shift is greater than a certain threshold). The white level of the arrows specifies the normalized magnitude of translation—brighter indicates relatively larger translation. The figures also display information about the standard deviation (SD) of the arrow lengths. This statistic gives a sense of the non-uniform translation of the image points across the image field. If all image points shift by the same amount, then the standard deviation will be zero. A larger value of the standard deviation indicates greater diversity in shifts, and hence greater distortion. In addition to the standard deviation, we also measure how much the centroid of the set

of points from the two images shifts. The translation of the centroid gives a sense of how the total image field "appear" to shift. However, we must note that we consider an image field to have *translated* only when *all* image points have at least a fixed minimum amount of shift in the direction of translation. Note that in all cases shown here, the *image points* were not determined using a "best focus" criterion, but rather by the point of intersection of the chief rays with the image plane. However, this definition of the *image* adopted for the current discussion does not limit the study of geometric properties, such as the kind of transformations induced by the rotations of the sensor and lens planes.

3.7.1 Properties of image field induced by sensor rotation ($\alpha_x,\ \alpha_y = 0,\ \beta_x, \beta_y \in \mathbb{R}$)

Figure 3.10 shows the images of the two object planes obtained under sensor rotation for three different values of pupil magnification. Studying the figures, we observe that:

1. The image plane is no longer frontoparallel with the object plane. As a result, the transverse magnification varies across the image field. Therefore, the image points undergo a field dependent and asymmetrical geometric distortion.
2. Since the location of both the entrance pupil and the exit pupil remain fixed, the on-axis image point continues to remain on-axis subsequent to the rotations. Therefore, we can conclude that the there is no translation of the image field following sensor rotation.
3. The amount of perspective distortion is directly proportional to the pupil magnification.
4. However, as shown in Figure 3.11, the distortion is independent of the object distance. Therefore, rotating the sensor plane does not introduce parallax between images that are obtained under varying orientations of the sensor. Consequently, if we capture multiple images under several rotations of the sensor, the inter-image homography—mapping between corresponding points of two images—is simply a perspective mapping of the following form:

$$H = \begin{bmatrix} a & b & 0 \\ d & e & 0 \\ g & h & 1 \end{bmatrix} \tag{3.28}$$

3.7.2 Properties of image field induced by lens rotation away from center of the entrance pupil ($\boldsymbol{\alpha_x},\ \boldsymbol{\alpha_y} \in \mathbb{R},\ \boldsymbol{\beta_x}, \boldsymbol{\beta_y} = \mathbf{0}; \boldsymbol{d_e} \neq \mathbf{0}$)

The influence of object distance and pupil magnification on the image shape obtained under lens rotation away from the entrance pupil is depicted in Figure 3.12. The emergence of parallax in the images is highlighted in Figure 3.13, in which we have plotted the top, middle and bottom rows of the image points for the three cases of pupil magnifications. We observe that:

1. The dominant effect of rotating the lens about a point along the optical axis is, in general, a *non-uniform shift* of the image field that depends on both the pupil magnification and object distance.
2. Since points in the image field undergo non-uniform translation, the standard deviation of the translation vector length is non-zero. Also, because the amount of shift of the image field is dependent on the object distance, the value of the standard deviation of the translation vector lengths is different for the images of the two object planes.
3. Since the amount of translation depends on the object distance, images obtained while varying rotation angle of the lens exhibit parallax as shown in Figure 3.13. We observe that in each case (of different pupil magnifications), the initially overlapping rows of the two images (from the two object planes) diverge with progressive rotation of the lens.
4. From the above observations, we infer that unless the pupil magnification is equal to one, the inter-image homography is a depth (object distance) dependent perspective mapping. In other words, for every object plane, the inter-image homography is of the form:

$$H(z_o) = \begin{bmatrix} a & b & c \\ d & e & f \\ g & h & 1 \end{bmatrix} \tag{3.29}$$

5. However, if the pupil magnification is equal to one, then the inter-image homography reduces to a depth dependent scaling transformation of the form:

$$H(z) = \begin{bmatrix} a & 0 & c \\ 0 & a & f \\ 0 & 0 & 1 \end{bmatrix} \tag{3.30}$$

3.7.3 Properties of image field induced by lens rotation about the center of the entrance pupil ($\boldsymbol{\alpha_x},\ \boldsymbol{\alpha_y} \in \mathbb{R},\ \boldsymbol{\beta_x}, \boldsymbol{\beta_y} = \mathbf{0};\ \boldsymbol{d_e} = \mathbf{0}$)

Finally, the properties of the image obtained when the lens is rotated about the center of the entrance pupil are depicted in Figure 3.14 and Figure 3.15. We observe that:

1. Rotation of the lens about the entrance pupil induces a shift of the image field, as must be expected.
2. However, unlike the previous case, the shift of the image field is *independent* of the object distance. We see that the standard deviation of the translation vector lengths is equal for both the group of points (from the two object planes).
3. Since the shift of the image field is independent of the object distance, there is no parallax between images obtained while rotating the lens about the entrance pupil. This is a very important property that can be used for several computational imaging techniques that rely on multiple image capture, including omnifocus imaging, digital super-resolution, panoramic imaging, etc.
4. If the pupil magnification is not equal to one, the inter-image homography is a *depth independent* perspective transformation of the form:

$$H = \begin{bmatrix} a & b & c \\ d & e & f \\ g & h & 1 \end{bmatrix} \tag{3.31}$$

5. If the pupil magnification is equal to one, then the inter-image homography is a depth independent perspective transformation of the form:

$$H = \begin{bmatrix} a & 0 & c \\ 0 & a & f \\ 0 & 0 & 1 \end{bmatrix} \tag{3.32}$$

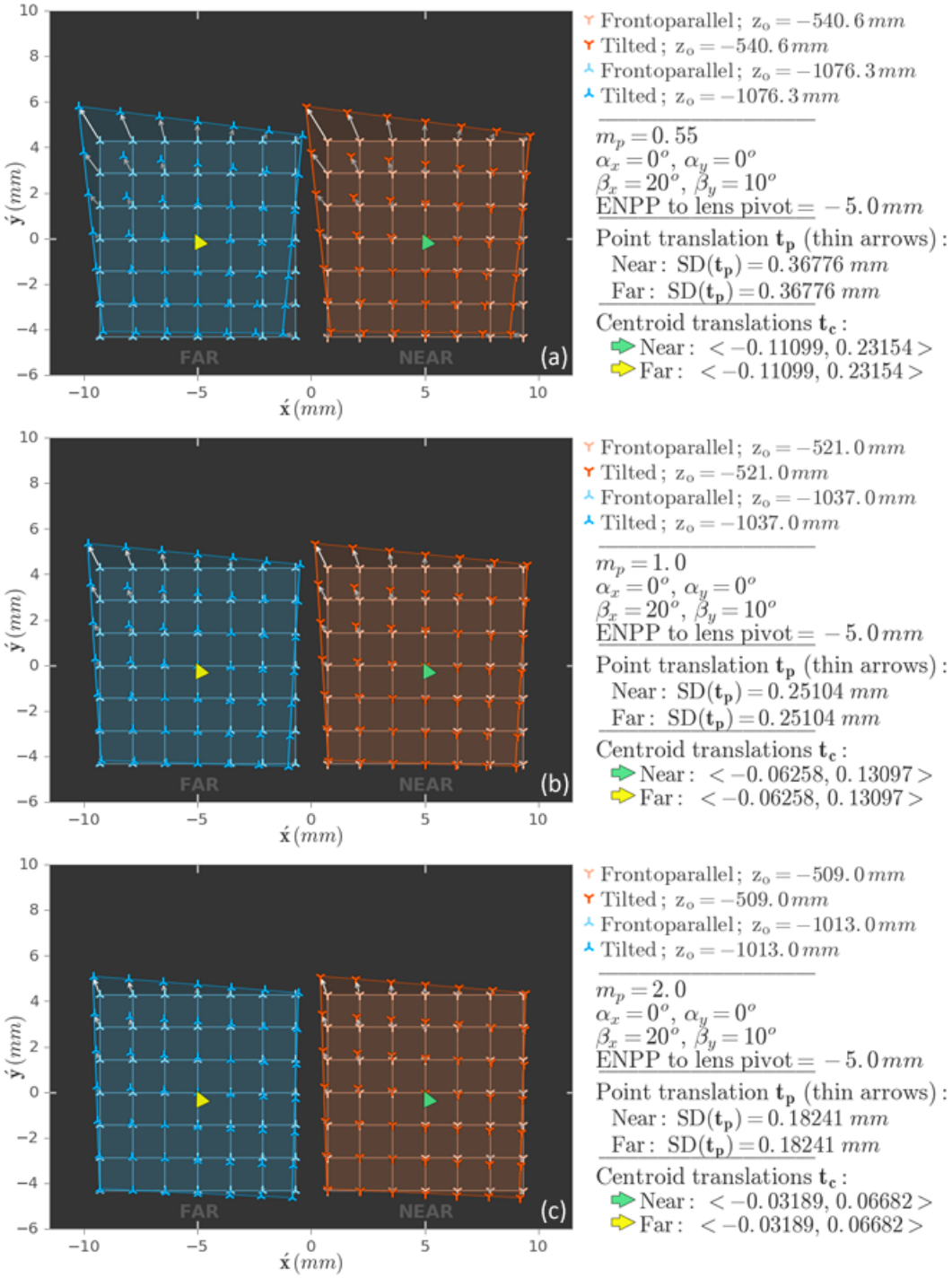

Figure 3.10 Geometric image under image plane (sensor) rotation for varying pupil magnifications. (a) $m_p = 0.55$, (b) $m_p = 1$, (c) $m_p = 2$.

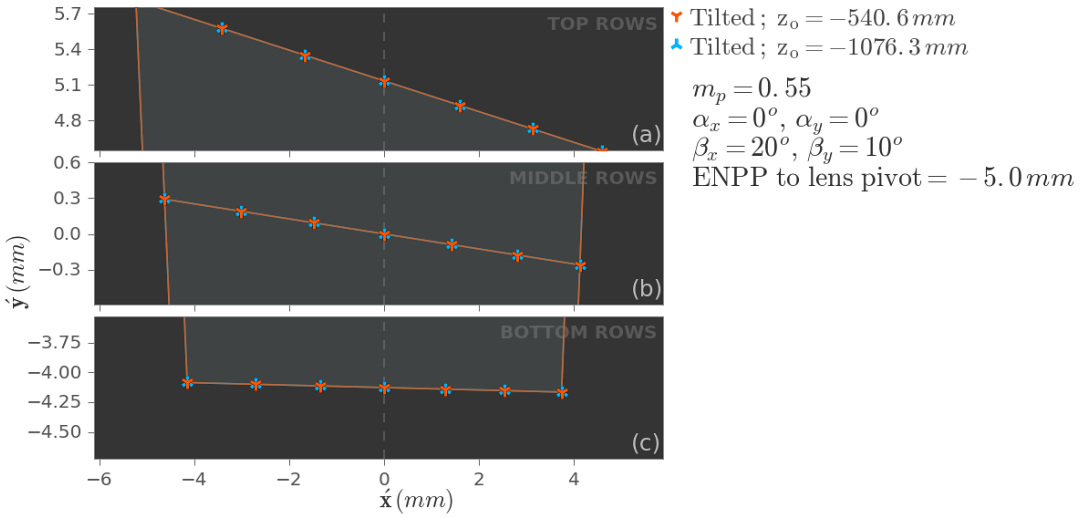

Figure 3.11 Comparison of geometric distortion induced by sensor rotation for varying object plane distances. The figure shows only the top, middle and bottom rows of image-points for pupil magnification $m_p = 0.55$ (Figure 3.10 (a)). Unlike in the previous figure, the two sets of image-points from the two object planes are left unseparated. We observe that the image-points corresponding to the two object planes that are at different distances from the lens experience the same type and amount of distortion. If that was not the case, then the image-point rows corresponding to the two planes would have diverged.

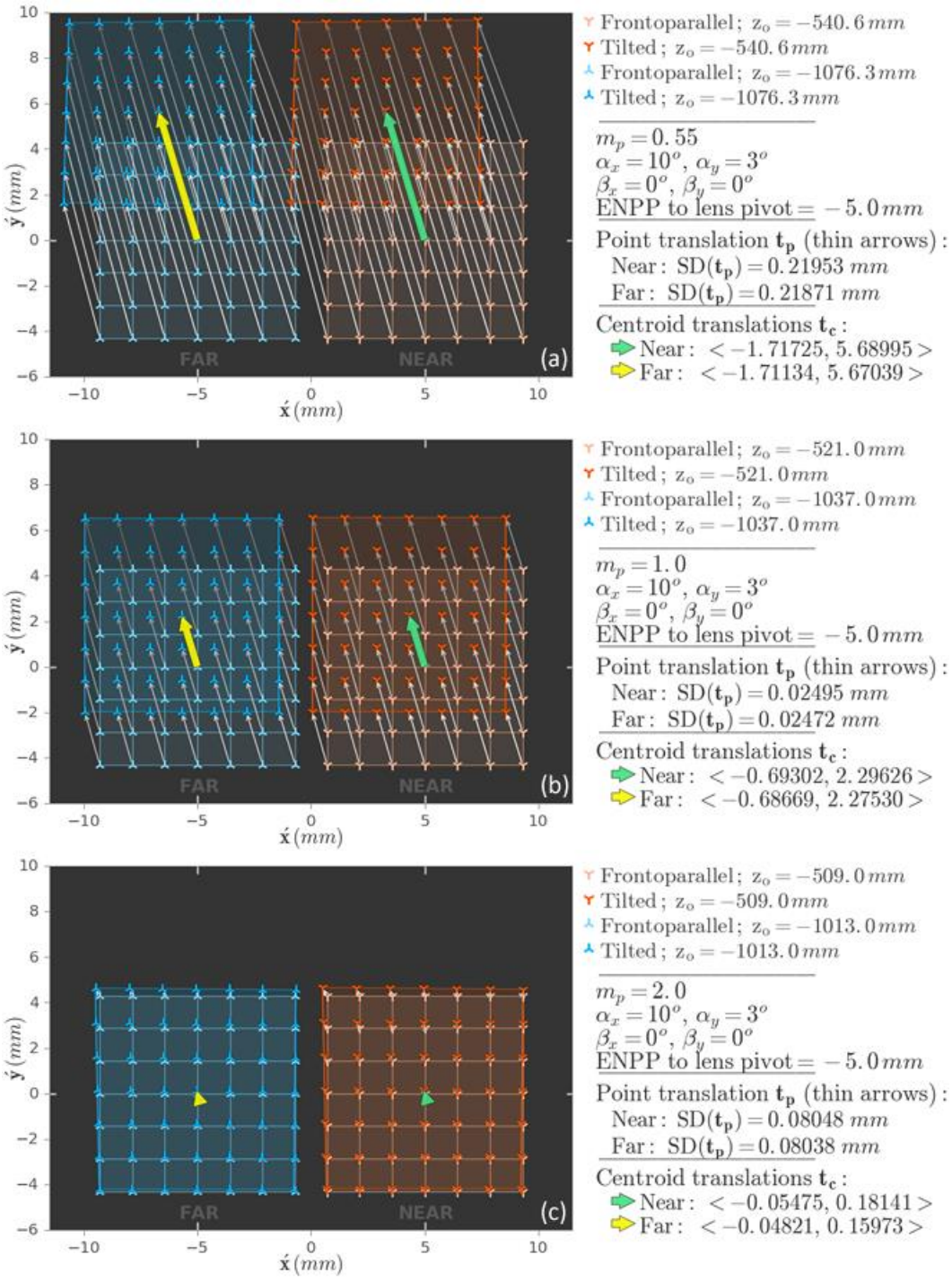

Figure 3.12 Geometric image under lens rotation away from the entrance pupil for varying pupil magnifications. (a) $m_p = 0.55$, (b) $m_p = 1$, (c) $m_p = 2$.

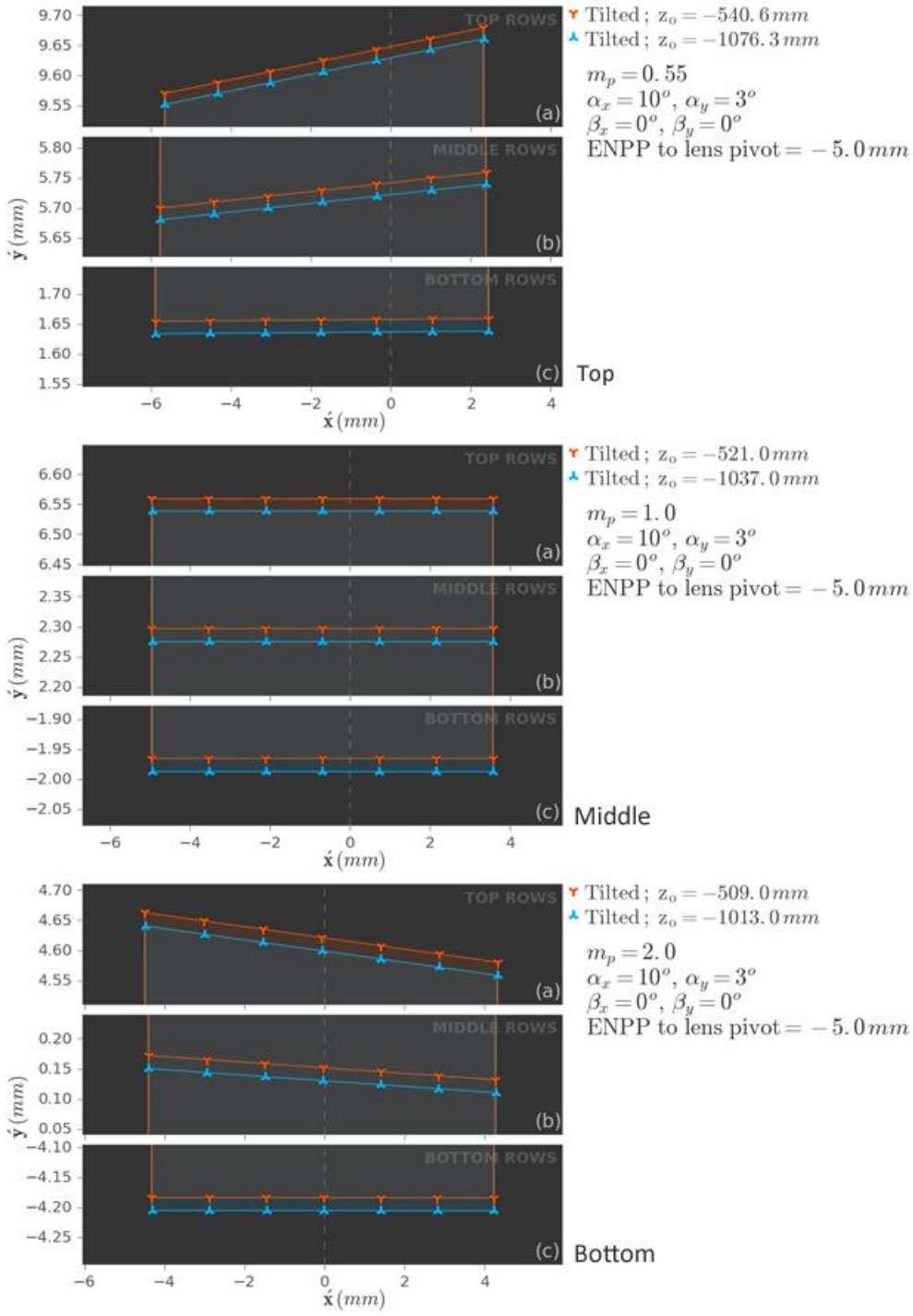

Figure 3.13 Variation of geometric distortion of image field induced by lens rotation away from the entrance pupil as a function of object distance and pupil magnification.

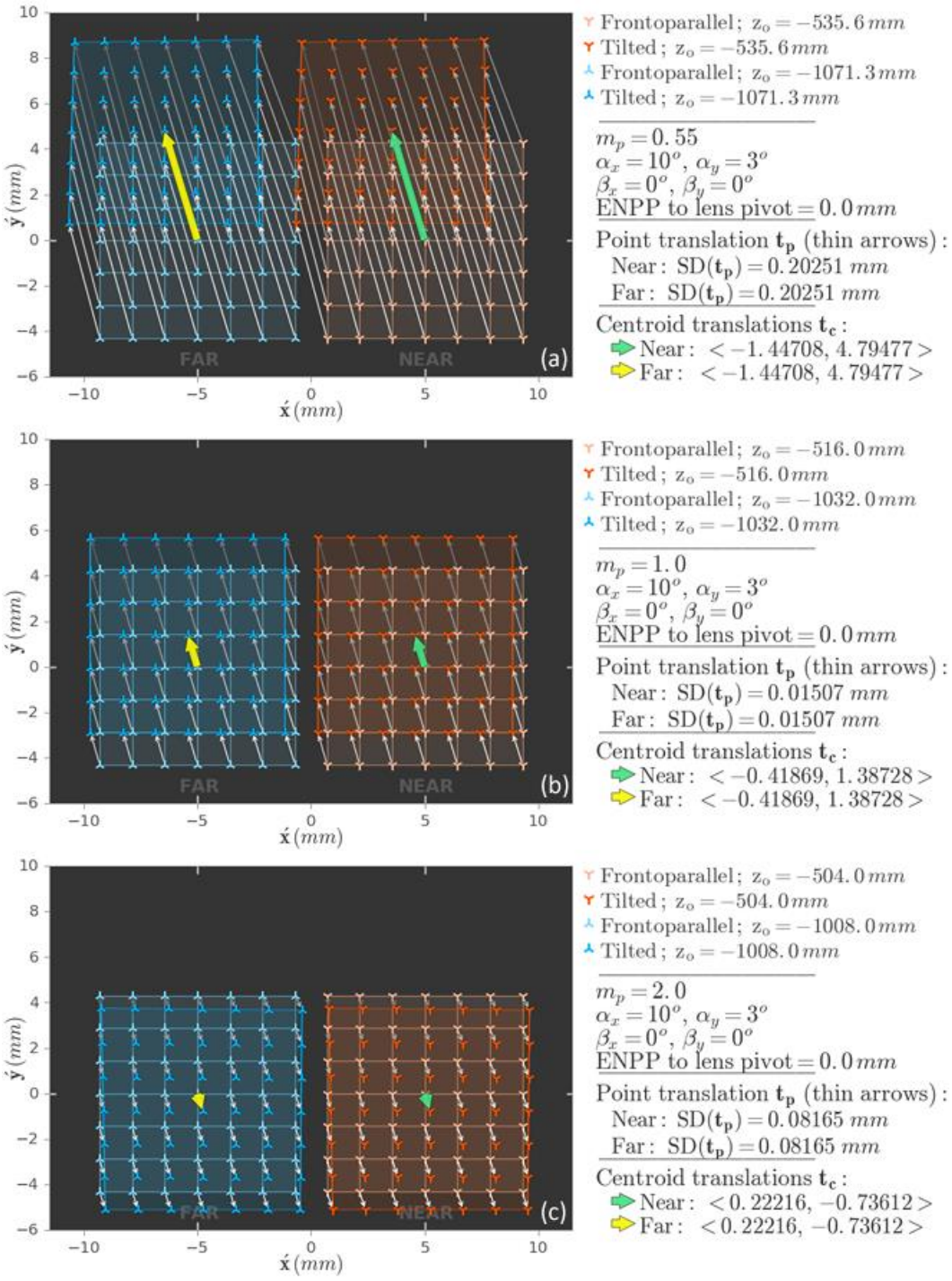

Figure 3.14 Geometric image under lens rotation away from the entrance pupil for varying pupil magnifications. (a) $m_p = 0.55$, (b) $m_p = 1$, (c) $m_p = 2$.

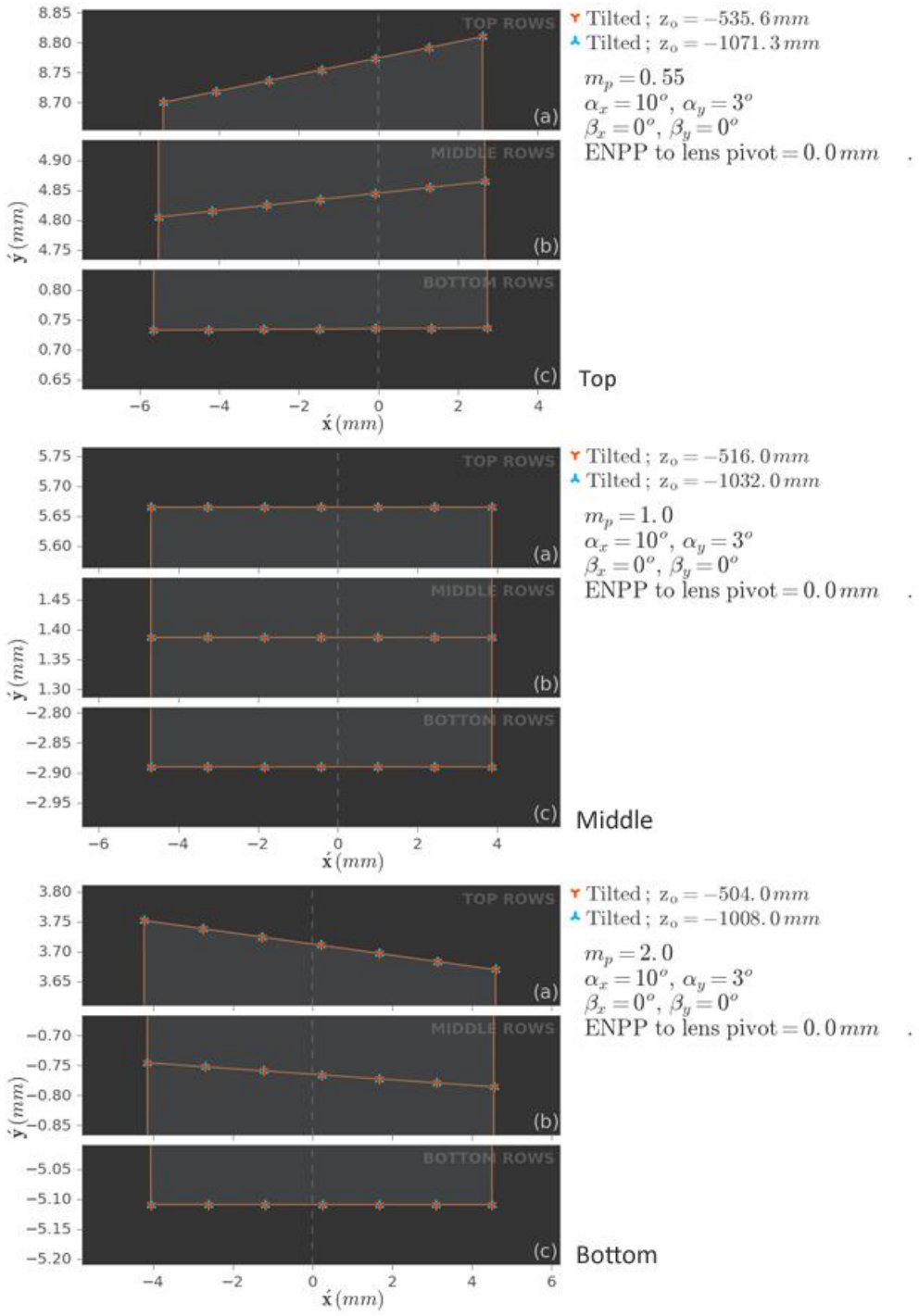

Figure 3.15 Variation of geometric distortion of images induced by lens rotation *about* from the entrance pupil as a function of object distance and pupil magnification.

3.8 Summary

The geometric relation between a three-dimensional object point (${}^{C}\mathbf{x}$) in camera coordinates and the corresponding image point (${}^{I}\acute{\mathbf{x}}$) in the two-dimensional image plane for an aberration-free Scheimpflug camera is given by Eq. (3.27):

$$ {}^{I}\acute{\mathbf{x}} = R_i{}^{T}\left(\acute{d}_e\,\boldsymbol{r}_{\ell,3} - \boldsymbol{t}_i\right) + \frac{\left(\widehat{\boldsymbol{n}}_i(3)\acute{z}_o - \acute{d}_e\widehat{\boldsymbol{n}}_i^{T}\,\boldsymbol{r}_{\ell,3}\right)}{\widehat{\boldsymbol{n}}_i^{T}R_\ell M_p R_\ell^{T}\left({}^{C}\mathbf{x} - d_e\,\boldsymbol{r}_{\ell,3}\right)}\,R_i{}^{T}R_\ell M_p R_\ell^{T}\left({}^{C}\mathbf{x} - d_e\,\boldsymbol{r}_{\ell,3}\right) $$

This imaging model has two important characteristics that differentiate it from other existing ones:

1. It is a most general geometric imaging relationship between object and image points for rectilinear imaging that accommodates the rotation of the image and the lens planes about their individual pivots. Common imaging models, such as for frontoparallel imaging, directly falls out of the above model.
2. The model incorporates optical parameters such as the pupil distances, pupil locations and pupil magnification, which enable us to accurately analyze the nature of the geometric image obtained the various possible orientation of the lens and image planes.

Our imaging model allowed us to study the effects of rotation of the lens and image planes on the geometric properties of the image. We discovered that if the pupil magnification m_p equal to one and the lens is rotated about the entrance pupil the inter-image homography—the transformation that relates the image of a scene obtained under varying rotations of the lens—is a simple composition of a scaling and translation transformations.

APPENDIX A

Appendix A.1 Transfer of chief ray's direction cosine for arbitrary orientation of the optical axis

In section 3.4 we derived the expression for the transfer of the chief ray's direction cosine from the entrance pupil to the exit pupil for a specific problem in which the optical axis was coincident with the z-axis of $\{C\}$. Furthermore, we inferred the general expression for the transfer relation—in which the optical axis is free to swivel about the origin of $\{C\}$—from the expression obtained for the specific problem. Here we apply the method of induction to formally derive the general expression.

Eq. (3.10) accurately represents the *transfer* for the specific problem; however, we will cast the expression in a slightly different form whose raison d'être is to enable generalization—through direct application of the result. Specifically, we express the output chief ray as a linear combination of the input chief ray and the optical axis; this is possible because the two rays and the optical axis span the same (meridional) plane. Let $\hat{\boldsymbol{c}}_z$, the standard basis vector along z-axis of $\{C\}$, represent the optical axis since the optical axis is coincident with the z-axis. Then,

$$\acute{\boldsymbol{l}} = w_1 \boldsymbol{l} + w_2 \hat{\boldsymbol{c}}_z \ , \qquad (A1.1)$$

where w_1 and w_2 are weights, and $\hat{\boldsymbol{c}}_z = [0, 0, 1]^T$.

Rewriting the above equation as

$$\begin{bmatrix} \acute{l} \\ \acute{m} \\ \acute{n} \end{bmatrix} = w_1 \begin{bmatrix} l \\ m \\ n \end{bmatrix} + w_2 \begin{bmatrix} 0 \\ 0 \\ 1 \end{bmatrix} \ , \tag{A1.2}$$

we can the readily obtain the weight w_1 by comparing equations Eq. (3.9) and Eq. $(A1.2)$ as:

$$w_1 = \pm \frac{1}{\sqrt{1 + (m_p^2 - 1)n^2}} \ . \tag{A1.3}$$

Substituting w_1 into $\acute{n} = w_1 n + w_2$ and comparing with Eq. (3.8) yields w_2 as:

$$w_2 = \pm \frac{(m_p - 1)n}{\sqrt{1 + (m_p^2 - 1)n^2}} \ . \tag{A1.4}$$

We are now ready to apply the result of the specific problem to the general problem. Figure 3.5 shows the schematic of the general problem—the optical axis pivots about the origin of $\{C\}$. Let us describe the general orientation of the optical axis by the action of the rotation matrix ${}^{c}R_{\ell} \in \mathbb{R}^{3\times3}$ on $\hat{\boldsymbol{c}}_z$. The matrix ${}^{c}R_{\ell}$ may be a composition of two or more matrices that denotes a sequence of rotations about the x-axis and y-axis. Then, $\hat{\boldsymbol{o}}$, the unit vector representing the new orientation of the optical axis, is obtained as the transformation of $\hat{\boldsymbol{c}}_z$ by the rotation matrix: $\hat{\boldsymbol{o}} = {}^{c}R_{\ell}\, \hat{\boldsymbol{c}}_z$ or $\hat{\boldsymbol{c}}_z = ({}^{c}R_{\ell})^{T} \hat{\boldsymbol{o}}$.

Since the output direction cosine $\acute{\boldsymbol{l}}$, the input direction cosine $\boldsymbol{l}$, and the optical axis $\hat{\boldsymbol{o}}$ lie on the same plane we can write $\acute{\boldsymbol{l}}$ as the linear combination of $\boldsymbol{l}$ and $\hat{\boldsymbol{o}}$:

$$\acute{\boldsymbol{l}} = w_1 \boldsymbol{l} + w_2 \hat{\boldsymbol{o}} \ . \tag{A1.5}$$

Note that the input direction cosine $\boldsymbol{l}$ in Eq. $(A1.5)$ (following the rotation of the optical axis) is, in general, different from the corresponding $\boldsymbol{l}$ in Eq. $(A1.1)$ even for the same object-point $\mathbf{x}$. This difference is due to the displacement of entrance pupil (E) following the rotation of the optical

axis; in fact, the designation of a ray as the chief ray (from **x** to E) alters as we displace the entrance pupil. Multiplying Eq. $(A1.5)$ by $({}^{c}R_{\ell})^{T}$, we obtain:

$$({}^{c}R_{\ell})^{T}\acute{\boldsymbol{l}} = w_1({}^{c}R_{\ell})^{T}\boldsymbol{l} + w_2({}^{c}R_{\ell})^{T}\hat{\boldsymbol{o}} \ . \tag{A1.6}$$

Letting $({}^{c}R_{\ell})^{T}\ \acute{\boldsymbol{l}} = \acute{\boldsymbol{l}}_R$ and $({}^{c}R_{\ell})^{T}\boldsymbol{l}\ = \boldsymbol{l}_R$, yields

$$\acute{\boldsymbol{l}}_R = w_1\boldsymbol{l}_R + w_2\hat{\boldsymbol{c}}_z \ . \tag{A1.7}$$

Comparing Eqs. $(A1.1)$ and $(A1.7)$, we obtain the expressions for the weights w_1 and w_2 as:

$$\begin{aligned} w_1 &= \pm\frac{1}{\sqrt{1+\left(m_p^2-1\right)n_R^2}}\ , \\ &\text{and} \\ w_2 &= \pm\frac{\left(m_p-1\right)n_R}{\sqrt{1+\left(m_p^2-1\right)n_R^2}}\ . \end{aligned} \tag{A1.8}$$

Where n_R represents the projection of the direction cosine vector, $\boldsymbol{l}$**,** on the rotated optical axis. If we write the matrix ${}^{c}R_{\ell}\ = [{}^{c}\boldsymbol{r}_{\ell,1}\quad {}^{c}\boldsymbol{r}_{\ell,2}\quad {}^{c}\boldsymbol{r}_{\ell,3}]$ where ${}^{c}\boldsymbol{r}_{\ell,i}$ for $i = 1, 2, 3$ are the columns of ${}^{c}R_{\ell}$, then:

$$({}^{c}R_{\ell})^{T} = \left[\left({}^{c}\boldsymbol{r}_{\ell,1}\right)^{T}\quad \left({}^{c}\boldsymbol{r}_{\ell,2}\right)^{T}\quad \left({}^{c}\boldsymbol{r}_{\ell,3}\right)^{T}\right]^{T}$$

and

$$\begin{aligned} \boldsymbol{l}_R &= ({}^{c}R_{\ell})^{T}\boldsymbol{l} \\ &= \left[\left({}^{c}\boldsymbol{r}_{\ell,1}\right)^{T}\quad \left({}^{c}\boldsymbol{r}_{\ell,2}\right)^{T}\quad \left({}^{c}\boldsymbol{r}_{\ell,3}\right)^{T}\right]^{T}\boldsymbol{l} \\ &= \left[\left({}^{c}\boldsymbol{r}_{\ell,1}\right)^{T}\boldsymbol{l}\quad \left({}^{c}\boldsymbol{r}_{\ell,2}\right)^{T}\boldsymbol{l}\quad \left({}^{c}\boldsymbol{r}_{\ell,3}\right)^{T}\boldsymbol{l}\right]^{T} \end{aligned}$$

Therefore, $n_R = \left({}^{c}\boldsymbol{r}_{\ell,3}\right)^{T}\boldsymbol{l}$ since n_R is the third element of $\boldsymbol{l}_R$.

Rewriting Eq. $(A1.7)$ as:

$$\begin{aligned}\acute{\boldsymbol{l}}_R &= \pm\frac{1}{\sqrt{1+\left(m_p^2-1\right)n_R^2}}\boldsymbol{l}_R \pm \frac{\left(m_p-1\right)n_R}{\sqrt{1+\left(m_p^2-1\right)n_R^2}}\hat{\boldsymbol{c}}_z \\ &= \pm\frac{1}{\sqrt{1+\left(m_p^2-1\right)n_R^2}}\left(\begin{bmatrix} l_R \\ m_R \\ n_R \end{bmatrix} \pm \left(m_p-1\right)n_R\begin{bmatrix} 0 \\ 0 \\ 1 \end{bmatrix}\right) \\ &= \pm\frac{1}{\sqrt{1+\left(m_p^2-1\right)n_R^2}}\underbrace{\begin{bmatrix} 1 & 0 & 0 \\ 0 & 1 & 0 \\ 0 & 0 & m_p \end{bmatrix}}_{\boldsymbol{M}_p}\begin{bmatrix} l_R \\ m_R \\ n_R \end{bmatrix}\end{aligned}$$

which can be compactly written as:

$$\acute{\boldsymbol{l}}_R = \pm\frac{1}{\sqrt{1+\left(m_p^2-1\right)n_R^2}}M_p\boldsymbol{l}_R \ . \qquad (A1.9)$$

Finally, substituting $({}^cR_\ell)^T\acute{\boldsymbol{l}} = \acute{\boldsymbol{l}}_R$ and $({}^cR_\ell)^T\boldsymbol{l} = \boldsymbol{l}_R$ yields the general expression for the direction cosines of the chief ray in the image space in terms of the pupil magnification and direction cosines in the object space as:

$$\acute{\boldsymbol{l}} = \pm\frac{1}{\sqrt{1+\left(m_p^2-1\right)n_R^2}}{}^cR_\ell M_p({}^cR_\ell)^T\boldsymbol{l} \ . \qquad (A1.10)$$

where $n_R = \left({}^c\boldsymbol{r}_{\ell,3}\right)^T\boldsymbol{l}$.

Appendix A.2 The direction cosine, originating from exit pupil, has unit ℓ^2-Norm

Claim: The direction cosine $\acute{\boldsymbol{l}}$ in the image space, obtained by the linear transformation of the direction cosine $\boldsymbol{l}$ in the object space, has unit ℓ^2-Norm, and $\{1+(m_p^2-1)n_R^2\}^{-1/2}$ is the normalization term.

Proof.

The expression for the direction cosine in the image space is

$$\acute{\boldsymbol{l}} = \frac{1}{\sqrt{1+(m_p^2-1)n_R^2}}\, {}^{c}R_{\ell} M_p ({}^{c}R_{\ell})^T \boldsymbol{l} \ . \qquad (A2.1)$$

where $n_R = \left({}^{c}\boldsymbol{r}_{\ell,3}\right)^T \boldsymbol{l}$, ${}^{c}\boldsymbol{r}_{\ell,i}$ is the i^{th} column of the rotation matrix ${}^{c}R_{\ell} \in \mathbb{R}^{3\times 3}$ applied to the optical axis, $\mathrm{M_p} = \begin{bmatrix} 1 & 0 & 0 \\ 0 & 1 & 0 \\ 0 & 0 & m_p \end{bmatrix}$, and $m_p \in \mathbb{R}^+$ is the pupil magnification.

Our objective is to prove $\left\|\acute{\boldsymbol{l}}\right\|^2 = 1$. For the convenience of notation within the proof, let

$$A = {}^{c}R_{\ell} M_p ({}^{c}R_{\ell})^T = Q \Lambda Q^T \ , \qquad (A2.2)$$

where $Q = {}^{c}R_{\ell}$, and $\Lambda = \mathrm{M_p}$, the diagonal matrix with non-negative real values.

Also, we represent the columns of Q as $\boldsymbol{q}_i = {}^{c}\boldsymbol{r}_{\ell,i}$ for $i = 1, 2, 3$. Then, $n_R = \left({}^{c}\boldsymbol{r}_{\ell,3}\right)^T \boldsymbol{l} = \boldsymbol{q}_3^T \boldsymbol{l}$, and

$$1 + (m_p^2 - 1)n_R^2 = 1 + (m_p^2 - 1)(\boldsymbol{q}_3^T \boldsymbol{l})^2 \ . \qquad (A2.3)$$

Since Q is a rotation matrix, it is orthonormal (the column of Q, having unit length, are orthogonal to each other). Therefore, $Q^T Q = Q Q^T = I$. Then,

$$\left\|\acute{\boldsymbol{l}}\right\|^2 = \frac{1}{1+\left(m_p^2-1\right)(\boldsymbol{q}_3^T\boldsymbol{l})^2}\|A\boldsymbol{l}\|^2 \quad , \tag{A2.4}$$

where

$$\begin{aligned}\|A\boldsymbol{l}\|^2 &= (A\boldsymbol{l})^T(A\boldsymbol{l}) \\ &= (Q\Lambda Q^T\boldsymbol{l})^T(Q\Lambda Q^T\boldsymbol{l}) \\ &= \boldsymbol{l}^T Q\Lambda^T Q^T Q\Lambda Q^T\boldsymbol{l} \\ &= l^T Q\Lambda^2 Q^T\boldsymbol{l} \\ &= \boldsymbol{s}\Lambda^2\boldsymbol{s}^T\end{aligned}$$

and $\boldsymbol{s} = Q^T\boldsymbol{l} = [\boldsymbol{q}_1^T\boldsymbol{l} \quad \boldsymbol{q}_2^T\boldsymbol{l} \quad \boldsymbol{q}_3^T\boldsymbol{l}]^T \in \mathbb{R}^{3\times 1}$ and $\boldsymbol{s}(i) = \boldsymbol{q}_i^T\boldsymbol{l} \in \mathbb{R}$.

Since Λ^2 is a diagonal matrix, we can rewrite $\|A\boldsymbol{l}\|^2$ as

$$\begin{aligned}\|A\boldsymbol{l}\|^2 &= \sum_{i=1}^{3}|s(i)|^2\Lambda^2(i,i) \\ &= (\boldsymbol{q}_1^T\boldsymbol{l})^2.1 + (\boldsymbol{q}_2^T\boldsymbol{l})^2.1 + (\boldsymbol{q}_3^T\boldsymbol{l})^2.m_p^2 \ .\end{aligned} \tag{A2.5}$$

Now,

$$\boldsymbol{s}^2 = \boldsymbol{s}^T\boldsymbol{s} = (Q^T\boldsymbol{l})^T(Q^T\boldsymbol{l}) = \boldsymbol{l}^T\boldsymbol{l} = 1 \quad (\because \|\boldsymbol{l}\|^2 = 1, \text{ by definition}) \ . \tag{A2.6}$$

Also,

$$\begin{aligned}\boldsymbol{s}^2 &= [\boldsymbol{q}_1^T\boldsymbol{l} \quad \boldsymbol{q}_2^T\boldsymbol{l} \quad \boldsymbol{q}_3^T\boldsymbol{l}]\begin{bmatrix}\boldsymbol{q}_1^T\boldsymbol{l}\\ \boldsymbol{q}_2^T\boldsymbol{l}\\ \boldsymbol{q}_3^T\boldsymbol{l}\end{bmatrix} \\ &= (\boldsymbol{q}_1^T\boldsymbol{l})^2 + (\boldsymbol{q}_2^T\boldsymbol{l})^2 + (\boldsymbol{q}_3^T\boldsymbol{l})^2 \\ &= 1 \quad (\because \boldsymbol{s}^2\text{=1, from above}) \ .\end{aligned} \tag{A2.7}$$

Substituting $(\boldsymbol{q}_1^T\boldsymbol{l})^2 + (\boldsymbol{q}_2^T\boldsymbol{l})^2 = 1 - (\boldsymbol{q}_3^T\boldsymbol{l})^2$ in Eq. $(A2.5)$ we obtain

$$\|A\boldsymbol{l}\|^2 = 1 - (\boldsymbol{q}_3^T\boldsymbol{l})^2 + (\boldsymbol{q}_3^T\boldsymbol{l})^2.m_p^2 = 1 + \left(m_p^2 - 1\right)(\boldsymbol{q}_3^T\boldsymbol{l})^2 \ . \qquad (A2.8)$$

Further, substituting $\|A\boldsymbol{l}\|^2$ into Eq. $(A2.4)$ we obtain

$$\begin{aligned} \left\|\acute{\boldsymbol{l}}\right\|^2 &= \frac{1}{1 + \left(m_p^2 - 1\right)(\boldsymbol{q}_3^T\boldsymbol{l})^2}\|A\boldsymbol{l}\|^2 \ . \\ &= 1 \end{aligned} \qquad (A2.9)$$

It follows that the scalar quantity $\frac{1}{\sqrt{1+(m_p^2-1)n_R^2}}$ is the normalization term. □

APPENDIX B

Appendix B.1 Derivation of Gaussian imaging equation with pupil magnification

The familiar Gaussian imaging equation, $-1/u + 1/\acute{u} = 1/f$, relates the object and image plane distances with the focal length f. In this formula, u is the *directed distance* (numerically negative as per our sign convention) between the object plane (perpendicular to the optical axis) and the principal plane (H) in the object space, $\acute{u}$ is the directed distance (numerically positive for *real* images) between the in-focus image plane and the principal plane ($\acute{H}$) in the image space. The distances u and $\acute{u}$ are measured along the optical axis.

If the distances of the object and image planes are specified with respect to the entrance (E) and exit ($\acute{E}$) pupil centers instead of the Principal planes, then the Gaussian lens formula needs to be modified. Here we derive the modified formula starting from the Gaussian lens formula. The same result was derived in [7] using a slightly different approach.

Figure B1.1 shows a schematic of the entrance and exit pupils, the object and image space Principal planes, and the object and image points. In the figure, u and $\acute{u}$ are the distances from the Principal planes to the object and image planes, e and $\acute{e}$ are distances from the Principal planes to the entrance- and exit-pupils, and z_e and $\acute{z_e}$ are the distances from the entrance- and exit-pupils to the object and image planes. Since the entrance- and exit-pupil planes are conjugates, like the object and image planes, the Gaussian lens formula holds as follows:

$$-\frac{1}{u}+\frac{1}{\acute{u}}=\frac{1}{f}\ , \qquad (B1.1)$$

and

$$-\frac{1}{e}+\frac{1}{\acute{e}}=\frac{1}{f}\ . \qquad (B1.2)$$

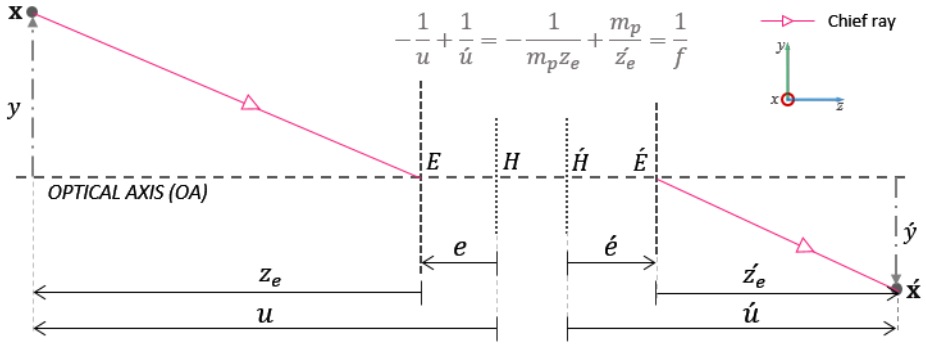

Figure B1.1 Schematic of imaging through a lens. The figure shows the object (y) and its image ($\acute{y}$), the object space principal plane (H) and the image side principal plane ($\acute{H}$), the entrance (E) and exit ($\acute{E}$) pupils, and the associated distances along the optical axis.

The transverse magnification m_t between the object and image planes is given as:

$$m_t=\frac{\acute{u}}{u}\ . \qquad (B1.3)$$

For images that are *real* and inverted, the transverse magnification m is numerically negative since the directed distance u is numerically negative, and $\acute{u}$ is numerically positive.

The pupil magnification m_p is defined as the ratio of the exit pupil diameter to the entrance pupil diameter. It is also the ratio between the exit pupil and entrance pupil distances (measured from the principal planes), just like the transverse magnification between any conjugate planes:

$$m_p=\frac{\acute{e}}{e}\ . \qquad (B1.4)$$

Equating Eqs. $(B1.1)$ and $(B1.2)$, we obtain

$$\frac{u-e}{eu} = \frac{\acute{u}-\acute{e}}{\acute{e}\acute{u}} \ .$$

Further, substituting $z_e = u - e$ and $\acute{z_e} = \acute{u} - \acute{e}$ in the above equation, and using Eqs. $(B1.3)$ and $(B1.4)$, we obtain a relationship between pupil magnification, transverse magnification, the object and image plane distances (specified with respect to the pupils) as:

$$\boxed{\frac{\acute{z_e}}{z_e} = \left(\frac{\acute{e}}{e}\right)\left(\frac{\acute{u}}{u}\right) = m_p m_t} \qquad (B1.5)$$

Substituting $u = z_e + e$ and $\acute{u} = \acute{z_e} + \acute{e}$ in Eq. $(B1.1)$ and equating with Eq. $(B1.2)$ yields

$$\frac{1}{\acute{z_e} + \acute{e}} - \frac{1}{z_e + e} = \frac{1}{\acute{e}} - \frac{1}{e} \ ,$$

which after cross-multiplication and cancellations of common terms produces

$$z_e \acute{z_e}(e - \acute{e}) + e^2 \acute{z_e} - \acute{e}^2 z_e = 0 \ .$$

Dividing by $z_e \acute{z_e} e\acute{e}$, and substituting $\frac{\acute{e}}{e}$ by the pupil magnification m_p, and $\left(\frac{e-\acute{e}}{e\acute{e}}\right)$ by $\frac{1}{f}$ we obtain:

$$\boxed{-\frac{1}{m_p z_e} + \frac{m_p}{\acute{z_e}} = \frac{1}{f}} \qquad (B1.6)$$

Where,

m_p	Pupil magnification.
z_e	Directed distance from the entrance pupil to the object plane.
$\acute{z_e}$	Directed distance from the exit pupil to the image plane.
f	Focal length.

Note that Eq. $(B1.6)$ is valid even if the z_e and $\acute{z_e}$ denote distances from the principal planes, provided we let $m_p = 1$. This outcome is indeed consistent with geometric optics theory, according to which the magnification between the principal planes is unity. In fact, Eq. $(B1.6)$ is more general than the Gaussian Lens formula in that it relates a pair of conjugate planes with any other pair of conjugate planes for which the transverse magnification (between the planes) is known. When one of the pairs happen to be the principal planes (H and $\acute{H}$) between which the magnification is one, we obtain the Gaussian Lens formula.

Finally, we also obtain the equations for computing the entrance- and exit-pupil distances from the respective principal planes by substituting Eq. $(B1.4)$ into Eq. $(B1.2)$ as

$$e = f\left(1 - \frac{1}{m_p}\right) ,$$
and
$$\acute{e} = f\left(m_p - 1\right) . \qquad (B1.7)$$

Appendix B.2 A brief account on the significance of pupil magnification

Although a pupil magnification close to one is a desirable property from the point of view of distortion in the presence of orientation misalignment, it seems to be hardly a critical design choice for most practical lenses except for those used for Scheimpflug photography as evident in plot of pupil magnifications in Figure B2.1. In addition, the figure shows that telephoto lenses have pupil magnification less one, and retrofocus wide-angle lenses have pupil magnification greater than one. The telephoto lenses employ a negative focal length group near the sensor plane to accommodate a long focal length lens into a compact body. Consequently, the exit pupil height (the image of the limiting aperture at the image side) is smaller compared to the entrance pupil height (the image of the limiting aperture at the object side). Therefore, in telephoto lenses the pupil magnification less

than one. On the other hand, a negative focal length group is placed at the front in short focal length, retrofocus lenses to create space between the lens and sensor which results in a larger exit pupil height compared to the entrance pupil height. Thus, the pupil magnification of retrofocus lenses are greater than one.

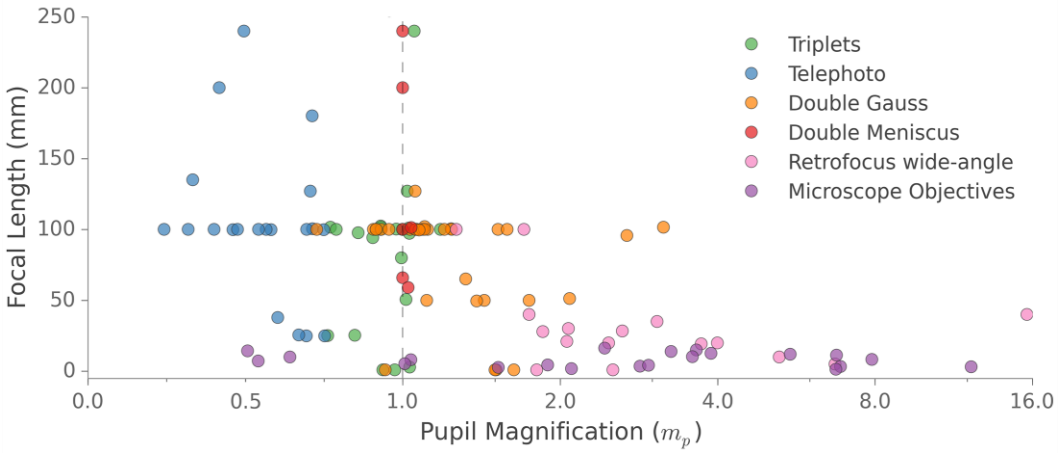

Figure B2.1 Pupil magnification m_p in a wide variety of lenses that form *real* images. The figure demonstrates the absence of any correlation between pupil magnification and focal length. In addition, only 20 in the sample 120 (or one in six) lenses have pupil magnification in the range 1 ± 0.05. Over 90% of all lenses have pupil magnification greater than 0.5. We obtained the samples from the Zemax Zebase library, which is a comprehensive catalogue of well-designed professional lenses.

The F-number (or F/#) is the ratio of the effective focal length f_E (distance between the image side Principal plane to the image plane with the object at infinity) to the paraxial entrance-pupil diameter D_e [11]

$$F/\# = \frac{f_E}{D_e} \ . \qquad (B2.1)$$

This infinite conjugate F/# is commonly specified by lens manufacturers on lens bodies.

The pupil magnification m_p is the ratio of the exit-pupil diameter $\acute{D}_e$ to the entrance-pupil diameter D_e:

$$m_p = \frac{\acute{D}_e}{D_e} \ . \qquad (B2.2)$$

Substituting $D_e = m_p \acute{D}_e$ from Eq. $(B2.2)(B1.2)$ into Eq. $(B2.1)$, we obtain

$$F/\# = \frac{m_p f_E}{\acute{D}_e} \ . \qquad (B2.3)$$

When the object is at infinity, the distance between the image plane and the exit pupil is obtained from Eq. $(B1.6)$ as

$$\acute{z_e} = m_p f_E \quad (\text{for } z_e = \infty). \qquad (B2.4)$$

Substituting $\acute{z_e}$ in place of $m_p f_E$ in Eq. $(B2.3)$ yields the alternative and equivalent definition for F-number—*as the ratio of the exit-pupil-to-image-plane distance to the exit-pupil diameter*:

$$F/\# = \frac{\acute{z_e}}{\acute{D}_e} \quad (\text{for } z_e = \infty), \qquad (B2.5)$$

where $\acute{z_e}$ is the distance from the exit pupil to the image plane, and $\acute{D}_e$ is the diameter of the exit pupil.

The F-number along with the wavelength λ determines the diffraction limited spatial resolution of optical imaging systems at the image plane as given by the equation:

$$r = \frac{1}{\lambda \, F/\#} \quad \text{lp/mm} \ . \qquad (B2.6)$$

For finite conjugate imaging, the object-plane-to-entrance-pupil distance decreases concomitant with an increase in exit-pupil-to-image-plane distance. This increase in the image plane distance effectively increases the F-number. The expression for the effective F-number in terms of the pupil magnification m_p is derived next.

Substituting $z_e = \frac{\acute{z_e}}{m_p\, m_t}$ (where m_t is the transverse magnification) from Eq. $(B1.5)$ into Eq. $(B1.6)$, followed by simple algebraic steps yields:

$$\acute{z_e} = f\left(m_p - m_t\right). \tag{B2.7}$$

We have established that the F-number (for infinite conjugate) is the ratio of the exit-pupil-to-image-plane distance to the exit pupil diameter. To obtain the effective F-number at finite conjugates, we substitute Eq. $(B2.7)$, the expression for the image-plane distance for finite conjugate imaging, into Eq. $(B2.5)$:

$$F/\#_{eff} = \frac{f\left(m_p - m_t\right)}{\acute{D}_e}\ . \tag{B2.8}$$

Further, substituting $\acute{D}_e = m_p D_e$ (Eq. $(B2.2)$) and replacing f/D_e with $F/\#$ we obtain:

$$F/\#_{eff} = F/\#\left(1 - \frac{m_t}{m_p}\right) \tag{B2.9}$$

where m_t is the transverse magnification (numerically negative for *real* images).

Now, we can obtain a more accurate equation for diffraction limited spatial resolution that is equally valid for both finite and infinite conjugate imaging by substituting Eq. $(B2.9)$ into Eq. $(B2.6)$

$$\boxed{r = \frac{1}{\lambda\, F/\#\left(1 - \frac{m_t}{m_p}\right)}\ \text{lp/mm}} \tag{B2.10}$$

where λ is the wavelength, $F/\#$ is the standard F-number defined for infinite conjugate imaging, m_p is the pupil magnification, and m is the transverse magnification (numerically negative for *real*

images). When the object is at infinity, $m_t = 0$ and Eq. $(B2.10)$ reduces to the optical resolution expression for infinite conjugate imaging.

REFERENCES

1. R. R. Shannon, *The Art and Science of Optical Design*, 1st Edition (Cambridge University Press, 1997).
2. R. Kingslake and R. B. Johnson, *Lens Design Fundamentals*, 2nd ed. (Academic Press, 2009).
3. J. P. Southall, *Mirrors, Prisms and Lenses, a Text-Book of Geometrical Optics*, Reprint edition (NY: Dover, 1964, 1964).
4. J. E. Greivenkamp, *Field Guide to Geometrical Optics* (SPIE Publications, 2003).
5. D. S. Goodman, "General principles of geometric optics," Handb. Opt. **1**, 1.23 (1995).
6. A. Walther, *The Ray and Wave Theory of Lenses*, 1st ed. (Cambridge University Press, 2006).
7. A. Hornberg, *Handbook of Machine Vision*, 1 edition (Wiley-VCH, 2006).
8. R. Hartley and A. Zisserman, *Multiple View Geometry in Computer Vision*, 2nd ed. (Cambridge University Press, 2004).
9. K. Devlin, *Mathematics: The Science of Patterns: The Search for Order in Life, Mind and the Universe*, 1st edition (Scientific American Library, 1997).
10. R. Szeliski, *Computer Vision: Algorithms and Applications*, 1st Edition. (Springer, 2010).
11. W. J. Smith, *Modern Optical Engineering*, 3rd ed. (McGraw-Hill Professional, 2000).